

DRAFT VERSION AUGUST 17, 2020

Typeset using L^AT_EX twocolumn style in AASTeX63

The Carnegie Supernova Project-I: Correlation Between Type Ia Supernovae and Their Host Galaxies from Optical to Near-Infrared Bands^{*}

SYED A UDDIN,^{1,2} CHRISTOPHER R. BURNS,¹ M. M. PHILLIPS,³ NICHOLAS B. SUNTZEFF,^{4,5} CARLOS CONTRERAS,³ ERIC Y. HSIAO,⁶ NIDIA MORRELL,³ LLUÍS GALBANY,⁷ MAXIMILIAN STRITZINGER,⁸ PETER HOEFLICH,⁶ CHRIS ASHALL,⁶ ANTHONY L. PIRO,¹ WENDY L. FREEDMAN,⁹ S. E. PERSSON,¹ KEVIN KRISCIUNAS,⁴ AND PETER BROWN⁴

¹Observatories of the Carnegie Institution for Science, 813 Santa Barbara St, Pasadena, CA, 91101, USA

²School of Science, Technology, Engineering and Math, American Public University System, 111 W. Congress Street, Charles Town, WV 25414, USA

³Carnegie Observatories, Las Campanas Observatory, Casilla 601, La Serena, Chile

⁴George P. and Cynthia Woods Mitchell Institute for Fundamental Physics and Astronomy, Texas A&M University, College Station, TX, 77843, USA

⁵Department of Physics and Astronomy, Texas A&M University, College Station, TX, 77843, USA

⁶Department of Physics, Florida State University, Tallahassee, FL 32306, USA

⁷Departamento de Física Teórica y del Cosmos, Universidad de Granada, E-18071 Granada, Spain

⁸Department of Physics and Astronomy, Aarhus University, Ny Munkegade 120, DK-8000 Aarhus C, Denmark

⁹Department of Astronomy & Astrophysics, University of Chicago, 5640 South Ellis Avenue, Chicago, IL 60637, USA

(Accepted August 17, 2020)

ABSTRACT

We present optical and near-infrared ($ugriYJH$) photometry of host galaxies of Type Ia supernovae (SN Ia) observed by the *Carnegie Supernova Project-I*. We determine host galaxy stellar masses and, for the first time, study their correlation with SN Ia standardized luminosity across optical and near-infrared ($uBgVriYJH$) bands. In the individual bands, we find that SNe Ia are more luminous in more massive hosts with luminosity offsets ranging between -0.07 ± 0.03 mag to -0.15 ± 0.04 mag after light-curve standardization. The slope of the SN Ia Hubble residual-host mass relation is negative across all $uBgVriYJH$ bands with values ranging between -0.029 ± 0.029 mag/dex to -0.093 ± 0.031 mag/dex — implying that SNe Ia in more massive galaxies are brighter than expected. The near-constant observed correlations across optical and near-infrared bands indicate that dust may not play a significant role in the observed luminosity offset–host mass correlation. We measure projected separations between SNe Ia and their host centers, and find that SNe Ia that explode beyond a projected 10 kpc have a 50% to 60% reduction of the dispersion in Hubble residuals across all bands — making them a more uniform subset of SNe Ia. Dust in host galaxies, peculiar velocities of nearby SN Ia, or a combination of both may drive this result as the color excesses of SNe Ia beyond 10 kpc are found to be generally lower than those interior, but there is also a diminishing trend of the dispersion as we exclude nearby events. We do not find that SN Ia average luminosity varies significantly when they are grouped in various host morphological types. Host galaxy data from this work will be useful, in conjunction with future high-redshift samples, in constraining cosmological parameters.

1. INTRODUCTION

Corresponding author: Syed A. Uddin
suddin@carnegiescience.edu

* This paper includes data gathered with the 6.5 meter Magellan Telescopes located at Las Campanas Observatory, Chile.

Since the surprising discovery of the accelerated expansion of the Universe (Riess et al. 1998, Perlmutter et al. 1997) using the standardization of SNe Ia (Phillips 1993, Tripp 1998), we have made little progress in understanding the physical cause of this observed acceleration. Although recent results tend to point towards a value consistent with the cosmological constant, other explanations are also possible (see Joyce et al. 2016). Alter-

native possibilities such as the time-varying nature of dark energy are currently difficult to test due to systematic uncertainties in deriving cosmological parameters (e.g., [Betoule et al. 2014](#), [Scolnic et al. 2017](#)). Along with improving photometric calibration, systematics of astrophysical origin need more attention. One such systematic is the interplay between the properties of SNe Ia and their hosts.

A number of studies have been made on the correlation between the properties of SNe Ia and their hosts ([Hamuy et al. 1995](#), [Sullivan et al. 2010](#), [Lampeitl et al. 2010](#), [Childress et al. 2013a](#), [Pan et al. 2014](#), [Uddin et al. 2017b](#), [Roman et al. 2018](#), [Wiseman et al. 2020](#)). These studies can be grouped into two categories: global host properties and local host properties (see [Uddin et al. 2017b](#) for a review). All studies, with varying degrees of significance, show that on average SNe Ia decline faster and are relatively over-luminous (i.e., more negative values of Hubble residuals¹) after light-curve standardization when hosted in massive galaxies. A few studies show correlations between SN Ia properties and SN Ia–host galaxy separation, as well as morphological types ([Wang et al. 1997](#), [Hicken et al. 2009](#), and [Galbany et al. 2012](#)). Some of these studies find that certain subgroups of SNe Ia can be better standard candles based on their host properties (e.g., [Rigault et al. 2013](#), [Kelly et al. 2015](#), [Uddin et al. 2017b](#)). Moreover, [Uddin et al. \(2017a\)](#) confirmed there is no bias in cosmological constraints derived from subsamples selected by host properties.

The correlation between SNe Ia luminosities and their hosts currently lacks explanation. A possible suspect is the effect of dust in the host galaxies ([Brout & Scolnic 2020](#)). One way to test this is to study SN Ia luminosity–host stellar mass correlations in multiple bands, preferably from optical to near-infrared. All previous studies, except [Burns et al. \(2018\)](#)², have used *B*-band peak brightness to study SN Ia–host correlations. In this study, we determine *ugriYJH* photometry and derive physical properties of host galaxies of SNe Ia from the *Carnegie Supernova Project-I* (hereafter CSP-I; [Hamuy et al. 2006](#)). Thereafter, we study the correlation of SN Ia Hubble residuals in *uBgVriYJH* bands with these properties. This paper is the first to study SN Ia

Hubble residual–host stellar mass correlations from optical to near-infrared wavelengths.

The CSP-I was designed to follow SNe Ia discovered at low redshifts, mostly from targeted transient search programs. The CSP-I performed photometric follow-ups over a wide range of bands from optical to near-infrared (*uBgVriYJH*), and was conducted between 2004–2010. Light-curves of SNe Ia from CSP-I are published in three papers ([Contreras et al. 2010](#), [Stritzinger et al. 2011](#), and [Kosciunas et al. 2017](#)). [Burns et al. \(2018\)](#) presented an absolute calibration of CSP-I SNe Ia photometry, and a new measurement of the Hubble constant. The second phase of the CSP (CSP-II) was conducted between 2011–2015, and the resulting SN Ia sample characteristics are described in [Phillips et al. \(2019\)](#) and in [Hsiao et al. \(2019\)](#). Optical and near-infrared Hubble diagrams from a combined SN Ia sample from CSP-I and CSP-II will be presented in a future paper (Uddin et al. in preparation). The purpose of this paper is to present the methodology of host mass determination and apply this to publicly available CSP-I data.

In § 2, we describe the SN Ia and host galaxy sample, § 3 describes host galaxy properties, and § 4 presents correlations between SNe Ia and hosts. A discussion of our findings is in § 5, and we summarize our conclusions in § 6.

2. DATA

2.1. SNe Ia Light-curves and Distances

We fit SN Ia light-curves using SNooPy ([Burns et al. 2011](#)). Briefly, the best-observed SNe Ia from the CSP-I are used as a training set to obtain light-curve templates for the set of *uBgVriYJH* filters as a function of a dimensionless color-stretch parameter s_{BV} , which is defined as the rest-frame time of maximum of the $B - V$ color-curve relative to time of *B*-band maximum divided by 30 ([Burns et al. 2014](#)). These templates are then used to fit the CSP-I sample of SNe Ia, resulting in estimates of s_{BV} , and magnitudes at maximum in each filter. Using the intrinsic colors from [Burns et al. \(2014\)](#), the reddening parameters $E(B - V)_{\text{host}}$ and R_V^{host} can also be determined. Finally, using the absolute magnitudes from [Burns et al. \(2018\)](#), we can infer distances and compute Hubble residuals. We describe details below.

Since we wish to investigate the behavior of Hubble residuals as a function of wavelength, it is important to minimize, as much as possible, the correlation between different filters. To this end, we fit each SN with

¹ Hubble residual is the difference between the predicted and the observed values of distance moduli after obtaining a best-fit cosmological model for a given set of SNe Ia. We will refer to Hubble residuals as luminosities in such a way that negative values indicate more luminous SNe Ia.

² We note that [Burns et al. \(2018\)](#) use 2MASS *K*-band photometry to determine host galaxy stellar mass: details in § 3.

SNooPy’s `max_model`. This model uses the light-curve shape templates as a function of color stretch s_{BV} to fit the maximum brightness $m_{max,\lambda}$ in each filter *independently*. However, the magnitudes are corrected for Milky Way extinction using the [Schlafly & Finkbeiner \(2011\)](#) dust maps, which introduces small correlated errors that are unavoidable. SNooPy also applies k-corrections computed using the [Hsiao et al. \(2007\)](#) SN Ia spectral sequence.

With these magnitudes at maximum in N filters, we can construct $N - 1$ independent colors at maximum. Using the methods from [Burns et al. \(2014\)](#), we use these colors to infer best-fit values for the host galaxy color excess $E(B - V)_{\text{host}}$ and reddening slope R_V^{host} for each SN. Again, this introduces some correlated errors due to the uncertainties in the extinction parameters which will be largest in the optical and smaller in the NIR. It is important that only colors are used to constrain the extinction. As shown in [Burns et al. \(2018\)](#), determining extinction by minimizing Hubble residuals leads to a significant bias in $E(B - V)_{\text{host}}$ and R_V^{host} .

Once the apparent magnitudes at maximum have been corrected for extinction, we compute absolute magnitudes using the luminosity distance³, μ_L (or Cepheid distance if available). We then fit these absolute magnitudes as a function of s_{BV} to obtain a luminosity-decline rate relation for each filter independently, using a 3rd-order polynomial (see [Burns et al. 2018](#)). To measure Hubble residuals, we use leave-one-out cross-validation: for each of the M SNe Ia, we use the other $M - 1$ to solve for the luminosity-decline rate relation. We use this to infer the distance to the SN that was left out, μ_{SN} . This inferred distance is subtracted from the μ_L to obtain the Hubble residual, $\mu_{\text{SN}} - \mu_L$ and we express it as $\Delta\mu$. The procedure is repeated for each filter and for all SNe.

Despite all these measures, there remains a large degree of correlation between the residuals of different filters. While most of this is due to the correlated brightness of the SNe themselves, at the median redshift of 0.025 for the CSP-I, an average peculiar velocity of 300 km/s would introduce an additional correlation of +/- 0.1 mag and could get as high as +/- 0.5 mag for our lowest-redshift objects. The latter can be mitigated by considering different redshift cuts. We attempt to mitigate this by considering different redshift cuts. We also attempt to remove the fastest decliners (for which the luminosity-decline rate relation corrections are largest) and the reddest objects (to reduce correlations due to extinction corrections). As we make more and more of these cuts, however, the statistical errors increase and we lose the ability to say anything definitive about the wavelength dependence of these mass effects (see subsection 4.2).

While the correlations due to peculiar velocity could be a cause for concern, we have no reason to believe they would be biased with respect to the mass of the host galaxy. They therefore introduce a significant level of white noise, but should not introduce a mass step/slope bias. Nevertheless, a more definitive answer will be possible using a sample like CSP-II that has a higher mean redshift ([Phillips et al. 2019](#)), is not as biased to high-mass galaxy hosts, and has sufficient numbers to allow selection cuts in decline rate and/or extinction.

The Hubble residuals of the CSP-I SN Ia sample used in this work are tabulated in Table A1. The following peculiar SNe Ia from the CSP-I are excluded: SN 2004dt, SN 2005gj, SN 2005hk, SN 2006bt, SN 2006ot, SN 2007so, SN 2008ae, SN 2008bd, SN 2008ha, SN 2008J, SN 2009dc, SN 2009J, and SN 2010ae (for details, see [Krisciunas et al. 2017](#)).

2.2. Host Galaxies

We obtain the list of host galaxies of CSP-I SNe Ia from [Krisciunas et al. \(2017\)](#). This is the final data release paper of CSP-I photometry and lists 123 SNe Ia in the redshift range of $0.004 < z < 0.083$. Host galaxy reference images were obtained at sufficiently later times so that no significant contribution of light from the SNe Ia contaminates the photometry. These were obtained primarily using the Tek5 optical CCD camera and the near-infrared WIRC (and RetroCam from 2011) on the 2.5 m Irène du Pont telescope, as well as with the SITE3 CCD camera and the near-infrared RetroCam on the 1 m Henrietta Swope telescopes at the Las Campanas Observatory. Some near-infrared images were also taken with the FourStar instrument on the 6.5 m Magellan Baade telescope. The reader is referred to [Krisciunas et al. \(2017\)](#) for further details.

In several cases, host identification of the SN Ia remains ambiguous. As described in detail in [Krisciunas et al. \(2017\)](#), the host galaxies of SN 2004gc, SN 2007A, SN 2007if, SN 2007mm, SN 2008bf, and SN 2008ff are unclear. These SNe Ia exploded within groups of galaxies where it is difficult to assign the true host, and so we

³ Luminosity distances are computed assuming a Hubble–Lemaître constant $H_0 = 72 \text{ km s}^{-1} \text{ Mpc}^{-1}$ and deceleration parameter $q_0 = -0.53$. For more details, see section 5.1 of [Burns et al. \(2018\)](#).

exclude them from this paper. Also, two SNe Ia share the same host: SN 2006mr and SN 2006dd. We exclude SN 2006dd since it was not observed by the CSP-I until very late epochs, making light curve fitting with SNooPy impossible. Finally, we exclude SN 2007sr as the host galaxy of this SN Ia is NGC 4038/NGC4039, also known as the Antennae Galaxies. SN 2007sr exploded in one of the tidal tails of this interactive pair (Schweizer et al. 2008), which makes it difficult to assign the correct host.

2.3. Host Galaxy Photometry

We measure apparent magnitudes of the host galaxies in each of the *ugriYJH* bands. Before performing photometry, we align all images with respect to the centers of each host galaxy, then co-add multiple exposures to make deeper images. We perform photometry using Source Extractor (SExtractor; Bertin & Arnouts 1996) in single image mode. We inspect SExtractor check images for failed detection and appropriate de-blending. Using calibrated local sequence stars, we determine zero points in each stacked image and compute apparent magnitudes of host galaxies using the MAG_AUTO magnitude definition of SExtractor.

As a check, we compare our optical photometry with the SDSS model magnitudes available from the SDSS Sky Server⁴, and with near-infrared photometry (*J* and *H*) from the 2MASS all-sky survey extended source catalog⁵. We show these comparisons in Fig. 1 and in Fig. 2, respectively. Slopes of best-fit relations and mean offsets with respect to CSP-I photometry are shown in Table 1.

Table 1. Slopes of best-fit relations and mean offsets when comparing CSP-I photometry with SDSS *ugri* photometry, and with 2MASS *JH* photometry.

Band	Slope	Offset (mag)
<i>u</i>	0.99	0.18
<i>g</i>	1.00	0.05
<i>r</i>	1.02	0.06
<i>i</i>	1.01	0.06
<i>J</i>	1.04	0.03
<i>H</i>	1.04	0.03

In some cases, when the host galaxy was not observed in a particular band by the CSP, photometry was obtained from external sources. For optical (*ugri*) filters, SDSS

model magnitudes⁶ were used, and for near-infrared (*J* and *H*), 2MASS extended source magnitudes were used. Offsets from Table 1 were applied to convert SDSS and 2MASS magnitudes to CSP-I system. We present photometry of the CSP-I SN Ia host galaxies in Table B1.

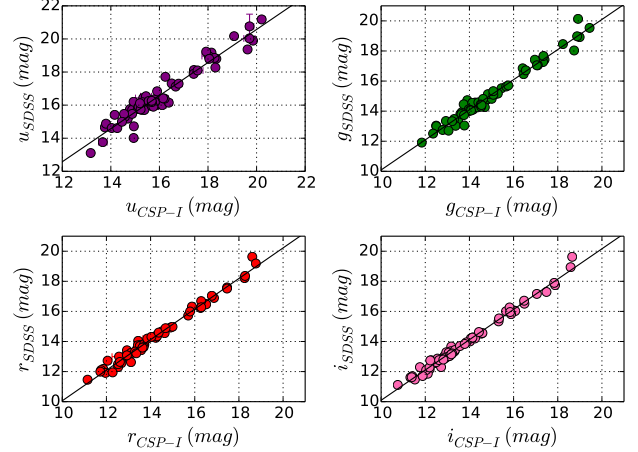


Figure 1. Comparison between host galaxy magnitudes from CSP and SDSS. In each case, solid lines are the best-fit linear relations to the data.

3. HOST GALAXY PROPERTIES

3.1. Stellar Mass

The physical properties of the host galaxies are derived by using the Z-PEG (Le Borgne & Rocca-Volmerange 2002) Spectral Energy Distribution (SED) software to fit the *ugriYJH* photometry. We follow the same procedure as described in Uddin et al. (2017b). Z-PEG uses the PEGASE 2.0 (Fioc & Rocca-Volmerange 1997) spectral libraries, and computes best matches using χ^2 minimization. There are nine galaxy templates: E, S0, Sa, Sb, Sbc, Sc, Sd, Im, and starburst. Additional internal extinction values are applied to each template ranging from 0.0 mag to 0.5 mag in steps of 0.05 mag. The Rana & Basu (1992) Initial Mass Function was adopted. The stellar masses of the CSP-I host galaxies are shown in Fig. 3 and presented in Table C1. The distribution has a peak at a relatively high mass, which is consistent with the fact that most SNe Ia were discovered by galaxy-targeted supernova searches (Hamuy et al. 2006). In contrast, host galaxies of SNe Ia from unbiased surveys

⁴ <https://skyserver.sdss.org/dr12/en/tools/search/IQS.aspx>

⁵ <http://tdc-www.harvard.edu/catalogs/tmxsc.html>

⁶ SDSS recommends the use of model magnitudes for extended objects and when color information, useful for stellar mass estimation, is preferred; details are in <https://www.sdss.org/dr12/algorithms/magnitudes/>

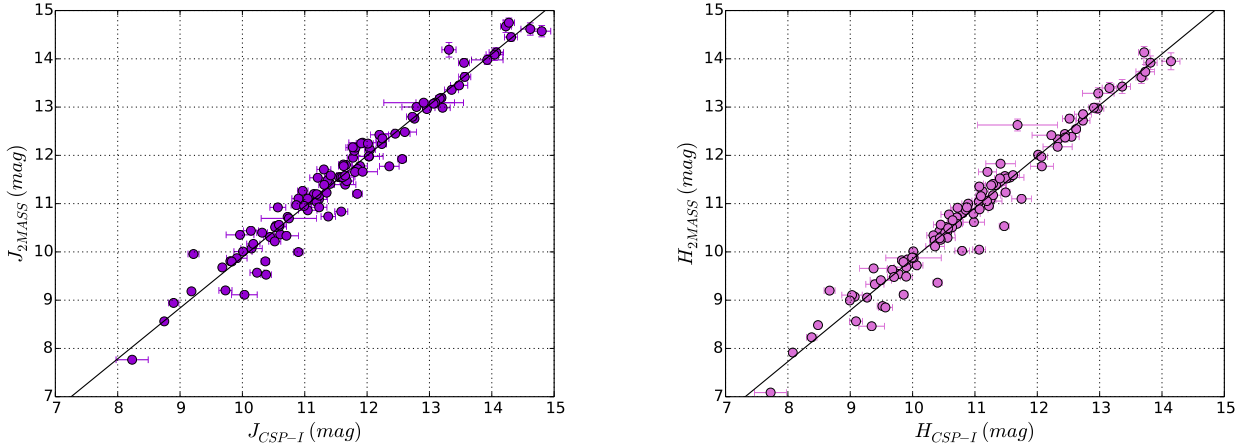


Figure 2. Comparison between host galaxy magnitudes from CSP-I and the 2MASS extended source catalog. In each case, solid lines are the best-fit linear relations to the data (see Eqn. 2).

have more low-mass galaxies (e.g., see figure 6 of Uddin et al. 2017b).

Kelly et al. (2010) demonstrated that galaxy stellar masses determined from multi-band photometry are in good agreement with those derived using galaxy spectra. They considered 10,000 galaxies from the SDSS and found an rms dispersion of 0.15 dex when they compared stellar masses derived using $ugriz$ photometry to those using spectral indices. Childress et al. (2013b) also performed a similar analysis and found similar dispersions when comparing 3673 galaxies.

Previously, Burns et al. (2018) calculated host galaxy stellar masses for the CSP-I SNe Ia using 2MASS K -band magnitudes. They utilized an empirical relation assuming a constant stellar mass-to-light ratio and normalized to the stellar masses from Neill et al. (2009). The host stellar masses that we calculate from this work are on average 0.3 dex lower than Burns et al. (2018). Comparing the host masses of 25 SNe Ia from this work that are in common with Neill et al. (2009), we find a mean difference of 0.18 dex. This comparison is shown in Fig. 4. It should be noted that Neill et al. (2009) used additional ultra-violet photometry from GALEX along with optical photometry in their analysis. Only 40% of the host galaxies in this work have photometry from GALEX. To maintain consistency we did not use GALEX data to derive host properties.

3.2. Separation Between SNe Ia and Hosts

We calculate the projected separation between SNe Ia and their hosts. First, we compute angular separations between SNe Ia and the center of their respective hosts. Then we calculate the distance to each SN Ia using red-

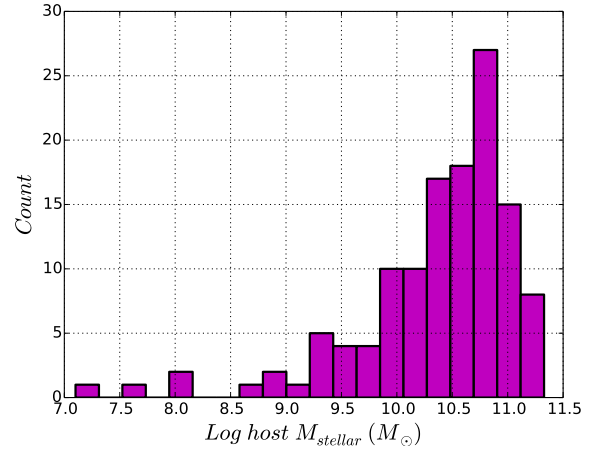


Figure 3. Distribution of host galaxy stellar mass of SNe Ia from CSP-I. The distribution has a peak at a relatively higher mass, which is a consequence of galaxy-targeted SN Ia searches.

shift and an assumed value of the Hubble-Lemaître constant, $H_0 = 70 \text{ km sec}^{-1} \text{ Mpc}^{-1}$. With these, we calculate a projected distance in kiloparsecs.

4. SN IA - HOST CORRELATIONS

4.1. $\Delta m_{15}(B)$ and s_{BV}

In this section, we present correlations between SNe Ia properties and their host galaxies. In Fig. 5 we show how B -band decline rate, $\Delta m_{15}(B)$ and s_{BV} correlate with host stellar mass. $\Delta m_{15}(B)$ is defined as the difference in magnitude of the B -band light-curve between maximum and day 15 in the rest-frame of the SN Ia (Phillips 1993). We do not see strong correlations, but as first noted by Sullivan et al. (2010), massive hosts

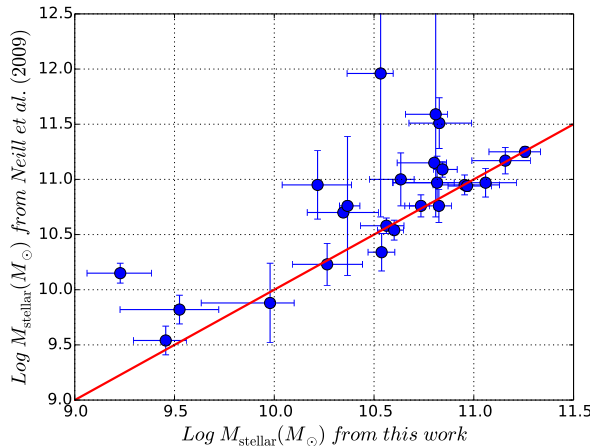


Figure 4. Comparison of host stellar masses from CSP-I and Neill et al. (2009). The solid line shows the one-to-one relation. Neill et al. (2009) determined, on average, 0.18 dex higher mass than what we calculate in this work. See text for discussion.

are observed to produce SNe Ia over the full range of decline rates, whereas less massive hosts preferentially give rise to slower declining events. We compare SN Ia light-curve properties with host galaxy ($g - r$) color in Fig. 6, where SN Ia properties are now on the horizontal axis. We reproduce the results in Hamuy et al. (2000) who found that fast declining SNe Ia are missing from blue galaxies with $(B - V) \leq 0.7$ mag, whereas galaxies with $(B - V) \geq 0.7$ mag produce SNe Ia with a wider range of decline rates. We see a similar pattern in our work, with the division occurring at $(g - r) \sim 0.6$ mag. We also find an excess of SNe Ia with higher values of s_{BV} (lower values of $\Delta m_{15}(B)$) occurring in bluer galaxies. Finally, we label galaxies with their morphological information obtained from NASA Extragalactic Database (NED)⁷. These classifications are available for 75% of CSP-I SN Ia host galaxies. Hamuy et al. (1995, 1996, 2000) found that spiral galaxies preferentially produce slower declining SNe Ia, whereas elliptical galaxies mostly host faster declining events. In order to test this, we perform a Kolmogorov-Smirnov (K-S) test to study possible intrinsic differences between the two populations of CSP-I SNe Ia: those exploding in spiral galaxies and those in elliptical or S0 galaxies. In terms of $\Delta m_{15}(B)$, the K-S test gives a value of 0.13 for D -statistics⁸ and a p -value of 0.47. For this value of D -statistics, the confidence level, $c(\alpha)$, is smaller than

0.005. Since p -value $\gg c(\alpha)$, we conclude that the two samples are likely drawn from the same population.

4.2. Hubble Residuals ($\Delta\mu$)

While the relations between $\Delta m_{15}(B)$ and s_{BV} with host properties are important from an astrophysical point of view (e.g., the explosion mechanism), SN Ia standardized luminosity variation with host stellar mass is important in deriving cosmological parameters (see Uddin et al. 2017b). In this section, we explore correlations between host stellar mass and SN Ia Hubble residuals for each of the $uBgVriYJH$ filters employed by the CSP-I, as shown in Fig. 7.

To quantify these correlations, we first calculate slopes of linear fits using a Bayesian method LINMIX (Kelly 2007), which takes into account the possibility of intrinsic scatter in the regression relationship along with possible correlated errors in both dependent and independent variables. Slopes are found to be negative across all filters, implying that SNe Ia in more massive galaxies are brighter than expected after standardizing the peak magnitudes using the luminosity–decline rate relation. The slope is least negative in V -band with a value of -0.029 ± 0.029 mag/dex and most negative in Y -band with a value of -0.093 ± 0.031 mag/dex. Table 2 summarizes the values of the slopes. While the slopes vary from filter to filter, these variations do not deviate significantly from a constant value.

Next, we split our sample into two groups at the median value of host stellar mass, $\log M_{\text{stellar}}(M_\odot) = 10.48$, and compute the weighted mean of Hubble residuals in each group. We find, on average, that SNe Ia that explode in a host at a higher mass than the median are over-luminous, after light-curve standardization. We call this the Hubble residual offset, Δ_{HR} . The offset varies across the filters, ranging from -0.074 ± 0.030 mag to -0.147 ± 0.040 mag. Table 2 summarizes the values of Δ_{HR} . Negative values of Δ_{HR} indicate that SNe Ia are more luminous in massive hosts. Note that the values of the slopes that we calculate are consistent within the uncertainties with those obtained by Burns et al. (2018).

SNe Ia in the nearby universe are affected by peculiar velocities, which in turn affects both SN Ia luminosities and host galaxy stellar mass in a correlated manner. We might, therefore, expect these correlations to change when nearby SNe Ia are excluded. Figures 8 and 9 display the correlations after excluding SNe Ia with redshifts $z < 0.005$ and $z < 0.01$, respectively. Table 2 summarizes the slopes and Δ_{HR} values obtained in different filters after applying these redshift cuts, with

⁷ <http://ned.ipac.caltech.edu>

⁸ D -statistics is the maximum difference between two cumulative distributions.

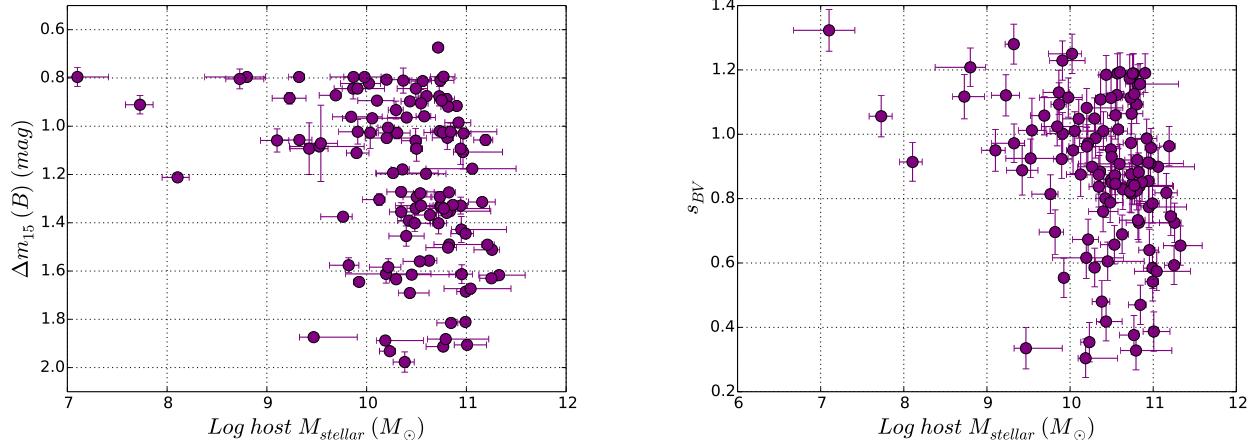


Figure 5. Distribution of $\Delta m_{15}(B)$ and s_{BV} with respect to their host stellar mass. See text for discussion.

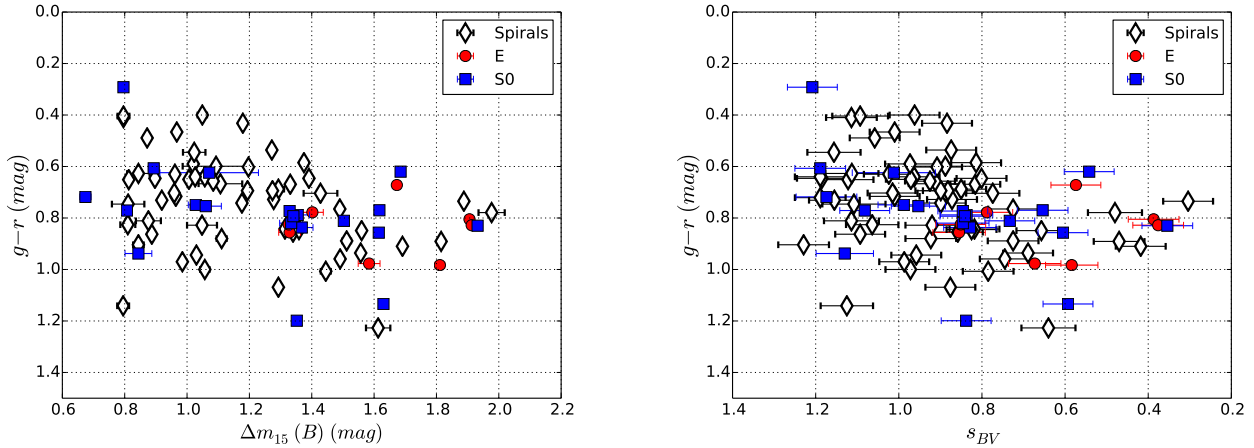


Figure 6. Distribution of $\Delta m_{15}(B)$ and s_{BV} with respect to their host $(g-r)$ color. See text for discussion.

the results displayed visually in Fig. 10. We find that the slopes shift towards positive values, but these shifts are not significant. The Δ_{HR} values change even less after excluding nearby SNe Ia.

Finally, we investigate two special cases. Typically, fast decliners and heavily reddened SNe Ia are not included in most cosmological analyses. To test how the SN Ia Hubble residual-host mass correlations might change by excluding these objects, we eliminate all SNe in the CSP-I sample with $s_{BV} > 0.5$ and $E(B-V) < 0.5$ mag. The resulting sample is plotted in Fig. 11 and slopes and Δ_{HR} are included in Table 2. We find small shifts in the values of the slopes and Δ_{HR} , but these are consistent within the errors with the values obtained for the full sample.

The CSP-I sample includes several SNe identified as 91T- and 91bg-like events. These classification are from

Folatelli et al. (2013), and are based on spectral comparison with SNID templates (Blondin & Tonry 2007). The Hubble residual-host mass correlations without these objects are plotted in Fig. 12, and the resulting slopes and Δ_{HR} values are included in Table 2. Again, we find only small shifts in these values.

It is important to note that the correlation between SN Ia Hubble residual and host galaxy stellar mass exists across all filters, *from optical to near-infrared wavelengths*. This implies that differences in the properties of the dust in low- and high-mass host galaxies is not likely the driving factor in these correlations, contrary to what is postulated by Brout & Scolnic (2020).

We further explore this in Fig. 13 where we plot the wavelength-dependence of Hubble residuals one would expect from the Brout & Scolnic (2020) model. These were estimated by randomly drawing a set of 100 color

excesses, $E(B - V)_{\text{host}}$, and values of the ratio of total to selective absorption, R_V^{host} , for a low-mass and high-mass sample consistent with the findings of Brout & Scolnic (2020). For $E(B - V)_{\text{host}}$ we drew from an exponential distribution with scale $\tau = 0.18$ mag for the high-mass sample and $\tau = 0.16$ mag for the low-mass sample. For R_V^{host} , we drew from a normal distribution with a mean $R_V^{\text{host}} = 1.5$ and standard deviation $\sigma_{R_V^{\text{host}}} = 0.8$ for the high-mass sample, and a mean $R_V^{\text{host}} = 2.5$ and $\sigma_{R_V^{\text{host}}} = 2.2$ for the low-mass sample. From these we computed, for each filter, the mean offset in luminosity that would result from assuming (incorrectly) there was a single average R_V^{host} for both samples. As is seen in Fig. 13, the resulting prediction for the behavior of the Hubble residual as a function of wavelength is not a good fit to the CSP-I observations.

4.3. Effect of SN Ia-Host Separation

We also investigate how Hubble residual varies as a function of the positions of the SNe in their host galaxies. This is displayed in Fig. 14 across the $uBgVriYJH$ filters. In Table 3, values of the dispersion in Hubble residuals for SNe Ia within 10 kpc of their host centers and for those beyond 10 kpc are tabulated for each filter. We find that SNe Ia exploding farther than 10 kpc from their host centers have a dispersion in Hubble residuals that is smaller than that for the SNe that explode within 10 kpc of their host centers. The reduction in the dispersion for the full sample varies from 50% to 60% across the filters. For the B band, which is representative of all the filters, the dispersion in Hubble residual for the SNe Ia beyond 10 kpc projected distance is ~ 0.17 mag smaller than the dispersion for the SNe Ia within 10 kpc.

We perform a Kolmogorov-Smirnov (K-S) goodness-to-fit test to study possible intrinsic differences between these two populations, one within 10 kpc projected distance, and the other beyond 10 kpc projected distance. The K-S test gives a value of 0.257 for D -statistics and a p -value of 0.218. For this value of D -statistics, the confidence level, $c(\alpha)$, is smaller than 0.001. Since p -value $\gg c(\alpha)$, we conclude that the two samples are likely drawn from the same population.

We note that there are 20 SNe Ia beyond 10 kpc from their host centers, perhaps causing an extra uncertainty due to small number statistics. To check this possible uncertainty and verify our finding, we perform a Monte Carlo simulation. The steps are: 1.) we first calculate the standard deviation of Hubble residuals for 20 SNe Ia that are beyond 10 kpc from their host centers; 2.) we randomly draw 20 SNe Ia Hubble residuals from

Table 2. Statistics on the SN Ia Hubble residual-host galaxy stellar mass correlation. Negative values in slopes indicate anti-correlation, i.e., SNe Ia are more luminous as host mass increases (see Fig. 7, 8, and 9). Errors in slopes and Δ_{HR} are in parentheses.

Sample	Filter	Slope (mag dex $^{-1}$)	Δ_{HR} (mag)
All	u	-0.076 (0.041)	-0.147 (0.044)
	B	-0.041 (0.031)	-0.089 (0.031)
	g	-0.032 (0.031)	-0.076 (0.028)
	V	-0.029 (0.029)	-0.074 (0.030)
	r	-0.041 (0.028)	-0.087 (0.029)
	i	-0.046 (0.030)	-0.085 (0.032)
	Y	-0.093 (0.031)	-0.137 (0.038)
	J	-0.078 (0.040)	-0.090 (0.046)
$z > 0.005$	u	-0.088 (0.040)	-0.156 (0.045)
	B	-0.039 (0.030)	-0.078 (0.031)
	g	-0.031 (0.029)	-0.068 (0.028)
	V	-0.026 (0.027)	-0.066 (0.030)
	r	-0.039 (0.027)	-0.078 (0.029)
	i	-0.045 (0.029)	-0.074 (0.032)
	Y	-0.090 (0.032)	-0.124 (0.038)
	J	-0.076 (0.042)	-0.064 (0.047)
$z > 0.01$	u	-0.072 (0.038)	-0.136 (0.047)
	B	-0.029 (0.027)	-0.089 (0.032)
	g	-0.024 (0.027)	-0.085 (0.027)
	V	-0.016 (0.024)	-0.076 (0.031)
	r	-0.030 (0.025)	-0.089 (0.031)
	i	-0.034 (0.026)	-0.080 (0.033)
	Y	-0.080 (0.031)	-0.122 (0.041)
	J	-0.074 (0.037)	-0.096 (0.051)
$s_{BV} > 0.5$ & $E(B-V)_{\text{host}} < 0.5$	u	-0.092 (0.038)	-0.166 (0.046)
	B	-0.031 (0.026)	-0.086 (0.031)
	g	-0.027 (0.025)	-0.083 (0.025)
	V	-0.022 (0.026)	-0.077 (0.031)
	r	-0.037 (0.027)	-0.090 (0.031)
	i	-0.046 (0.027)	-0.096 (0.033)
	Y	-0.084 (0.032)	-0.142 (0.042)
	J	-0.078 (0.039)	-0.103 (0.050)
Exclude 91T- & 91bg-like SNe Ia	u	-0.061 (0.038)	-0.099 (0.045)
	B	-0.036 (0.030)	-0.063 (0.031)
	g	-0.028 (0.029)	-0.051 (0.028)
	V	-0.025 (0.028)	-0.052 (0.031)
	r	-0.038 (0.028)	-0.061 (0.030)
	i	-0.041 (0.029)	-0.060 (0.033)
	Y	-0.087 (0.033)	-0.118 (0.040)
	J	-0.080 (0.039)	-0.080 (0.049)
	H	-0.035 (0.036)	-0.067 (0.046)

SNe Ia that are within 10 kpc from their host centers and calculate the standard deviation; and 3.) we compare

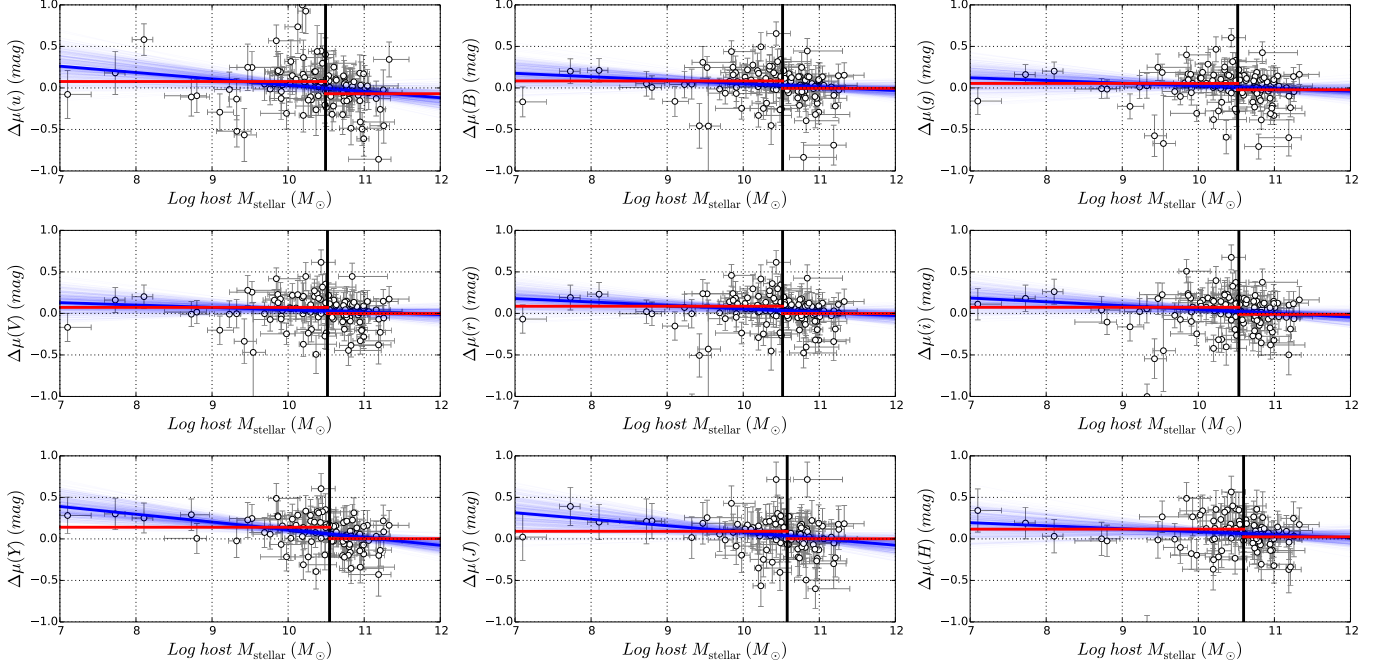


Figure 7. SN Ia Hubble residual ($\Delta\mu$) vs host stellar mass across $uBgVriYJH$ bands. In each case, the vertical solid black line shows the median split point, the slanted blue thick solid line shows the best-fit linear trend with lighter blue lines contain the 95% pointwise confidence intervals on the regression line, and red solid lines show the weighted mean of Hubble residuals at both sides of the split point. Slopes of the best-fit lines and Hubble residual offsets are presented in Table 2.

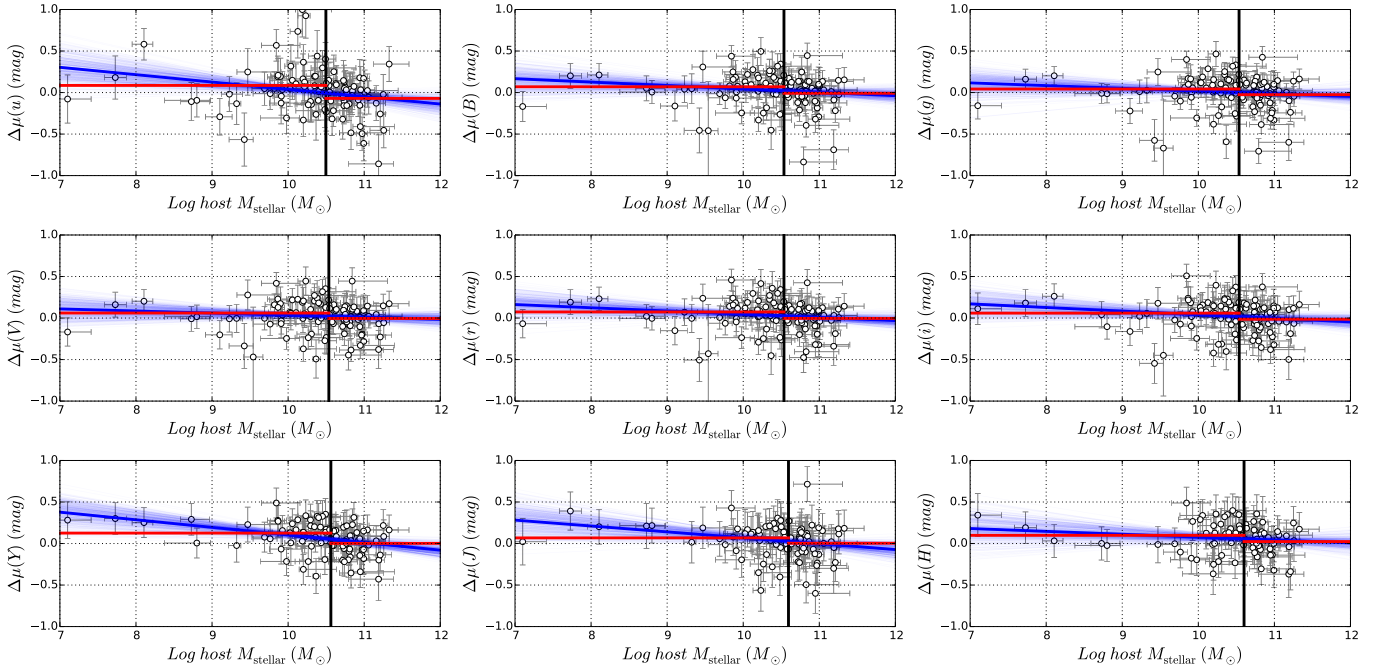


Figure 8. Same as Fig. 7 but including only SNe Ia with $z > 0.005$.

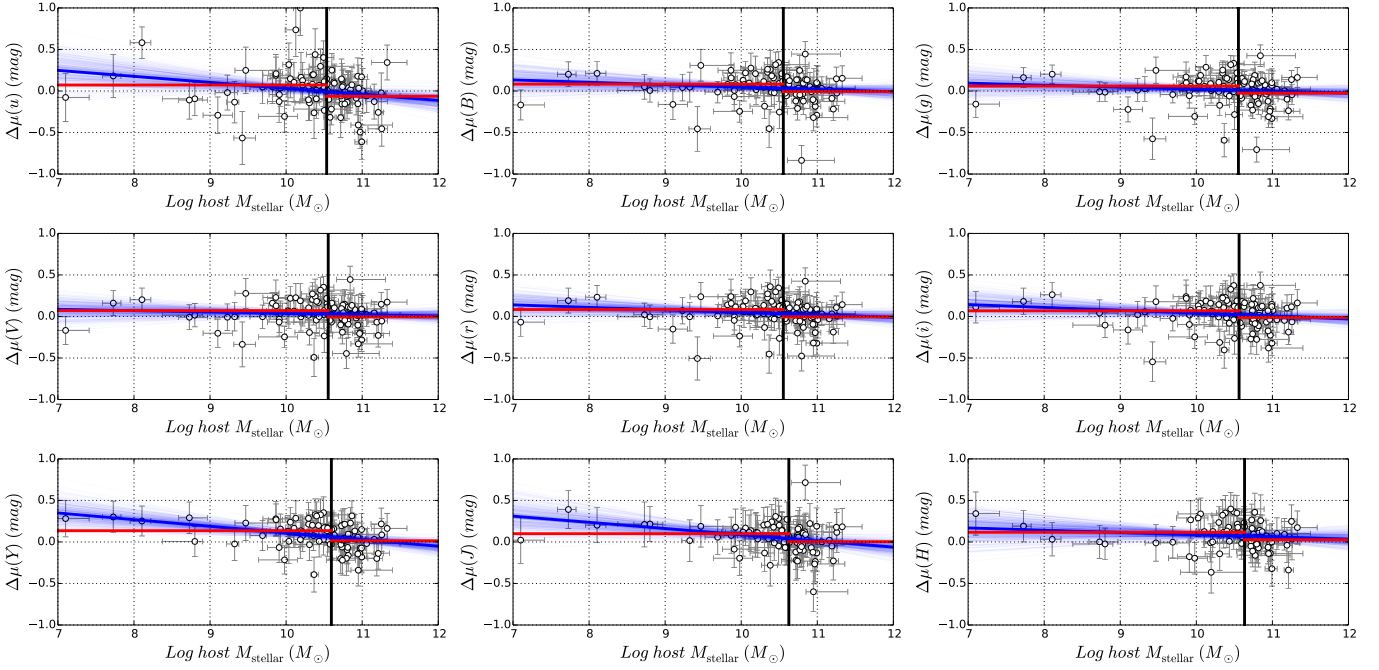


Figure 9. Same as Fig. 7 but including only SNe Ia with $z > 0.01$.

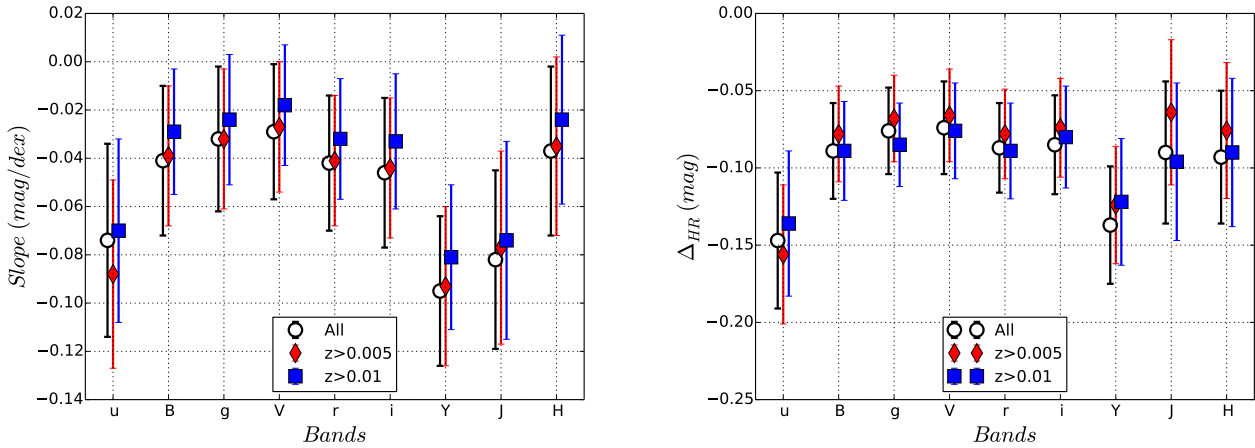


Figure 10. Variation of slope (left) and Δ_{HR} (right) in different bands. They are shown for the parent sample, $z > 0.005$ sample, and $z > 0.01$ sample. See Table 2 for the values of slopes and Δ_{HR} .

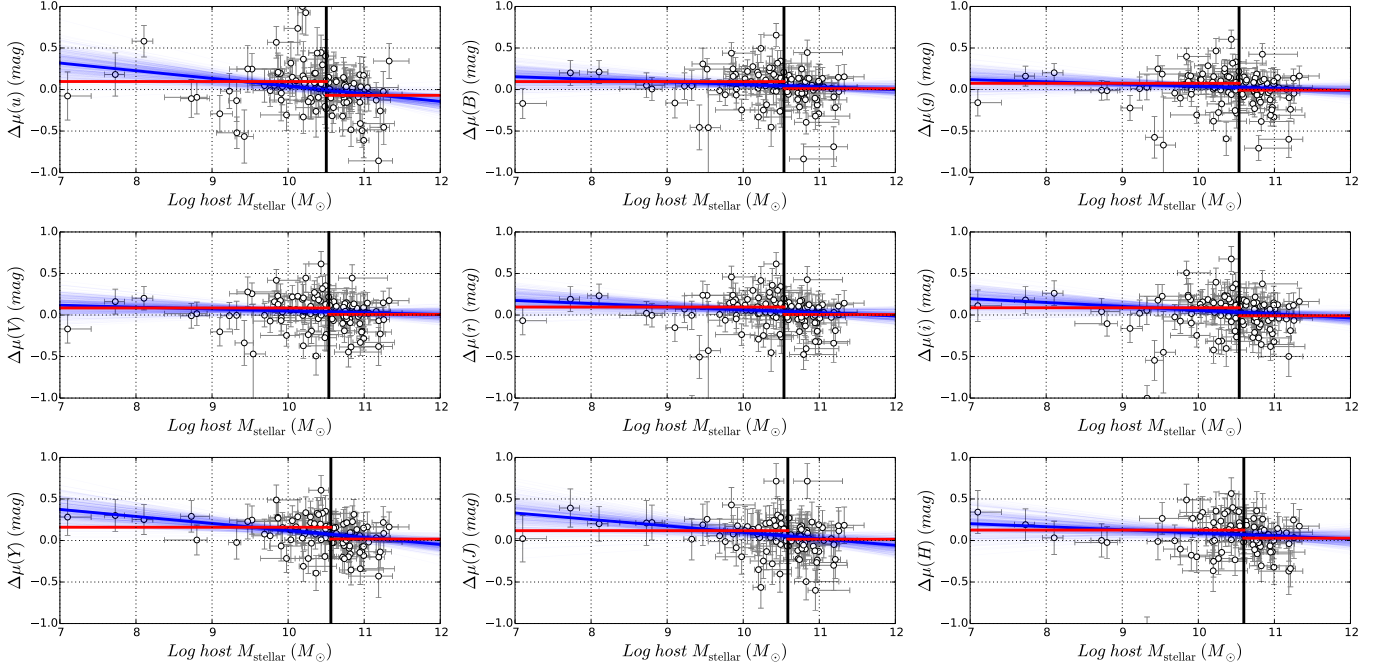


Figure 11. Same as Fig. 7 but including only SNe Ia with $s_{BV} > 0.5$ and $E(B-V) < 0.5$.

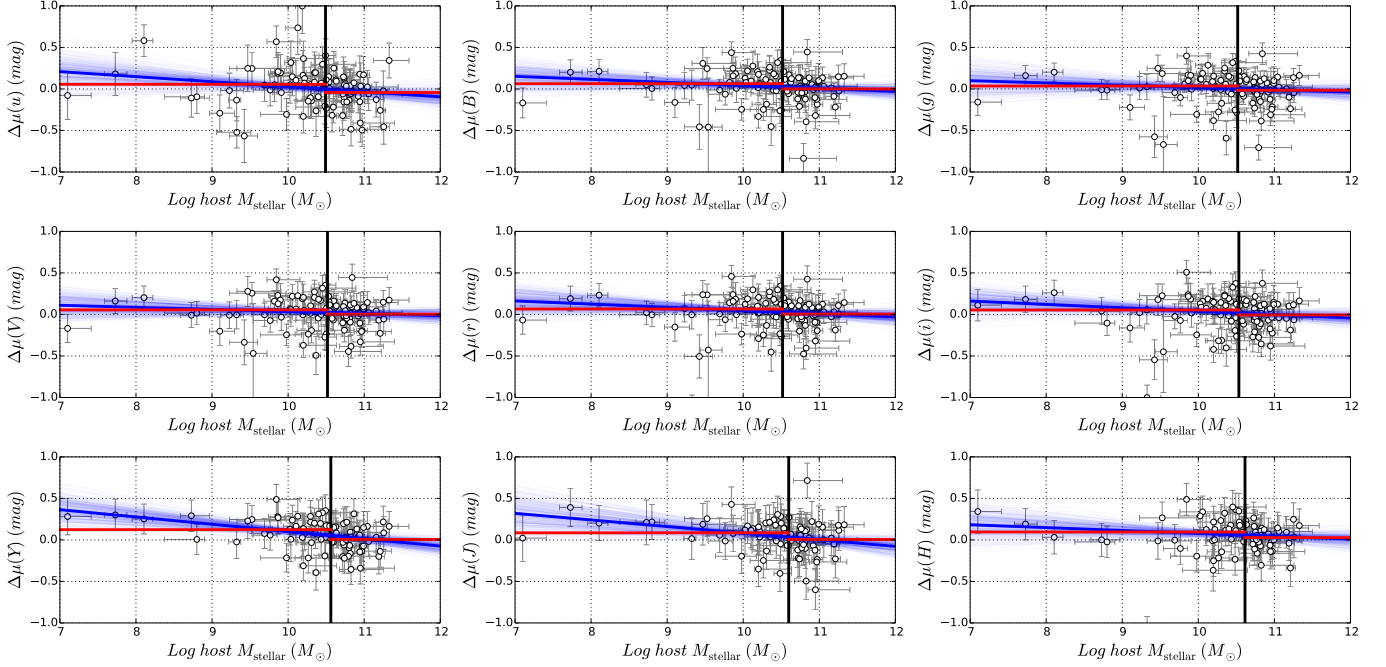


Figure 12. Same as Fig. 7 but excluding 91T- and 91bg-like SNe Ia.

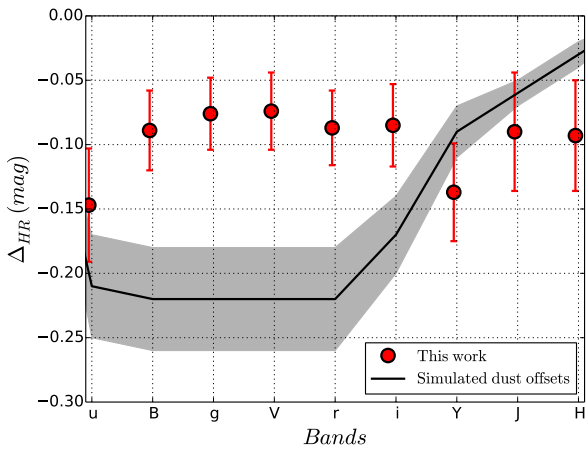


Figure 13. Similar to Fig. 10 (right) but adding simulated dust offsets according to Brout & Scolnic (2020). See subsection 4.2 for discussion.

the standard deviations of the Hubble residuals found in steps 1 and 2. After running a million Monte Carlo realizations in this manner, the mean of the differences in the standard deviations is found to be 0.12 ± 0.03 mag. This implies that the result we have found did not occur by chance.

To check if the peculiar velocities of nearby SNe Ia have an effect, we recalculate the dispersions in Hubble residual for SNe Ia at $z > 0.005$ and at $z > 0.01$ (see Table 3). For SNe Ia at redshifts $z > 0.005$ there is no appreciable change in their dispersions across the wavelengths compared to the full sample. But if we limit the sample to those at redshifts $z > 0.01$, a ~ 0.07 mag decrease in the dispersions for SNe Ia within 10 kpc is observed in all filters except u . Note, also, that the differences in the dispersions for the SNe beyond 10 kpc compared to those within 10 kpc grow smaller and tend to decrease with wavelength. This suggests that a combination of peculiar velocities and small errors in host dust corrections may be responsible for the observed difference in dispersion for SNe Ia within 10 kpc versus those beyond 10 kpc from the centers of their hosts.

Finally, looking at the host galaxy mass distribution, we find that for the inner sample (< 10 kpc), 75% of the hosts are massive ($\log M_{\text{stellar}}(M_{\odot}) > 10$), whereas for the outer sample (> 10 kpc), 88% of the hosts are massive. Hence, there is a small excess (13%) of massive host galaxies for SNe Ia that explode beyond 10 kpc from their host centers.

5. DISCUSSION

Table 3. Dispersion in Hubble residuals of SNe Ia that are within 10 kpc from their host centers and those that are beyond 10 kpc in various bands.

Filter	Dispersion in $\Delta\mu$ (mag)	
	Distance < 10 kpc	Distance > 10 kpc
All		
u	0.34	0.16
B	0.27	0.10
g	0.27	0.11
V	0.25	0.10
r	0.25	0.10
i	0.25	0.12
Y	0.25	0.12
J	0.28	0.12
H	0.25	0.15
$z > 0.005$		
u	0.34	0.16
B	0.26	0.10
g	0.27	0.11
V	0.24	0.10
r	0.24	0.10
i	0.24	0.12
Y	0.25	0.12
J	0.27	0.12
H	0.24	0.15
$z > 0.01$		
u	0.31	0.14
B	0.20	0.10
g	0.20	0.11
V	0.18	0.10
r	0.18	0.10
i	0.18	0.12
Y	0.17	0.13
J	0.20	0.12
H	0.18	0.15

- (a) Our results on the correlation between SN Ia Hubble residual and host stellar mass are consistent with other published studies. When we compare our results with previous studies we find that results vary in magnitude (and significance) due to different sample size and analysis. Except for Burns et al. (2018), all previous studies used B -band Hubble residuals. Pan et al. (2014) studied the SN Ia Hubble residual-host mass correlation with a sample of 50 SNe Ia from the Palomar Transient Factory. They found a value of Δ_{HR} of -0.08 ± 0.04 mag, and a slope of -0.041 ± 0.030 mag dex $^{-1}$. Childress et al. (2013a) used 115

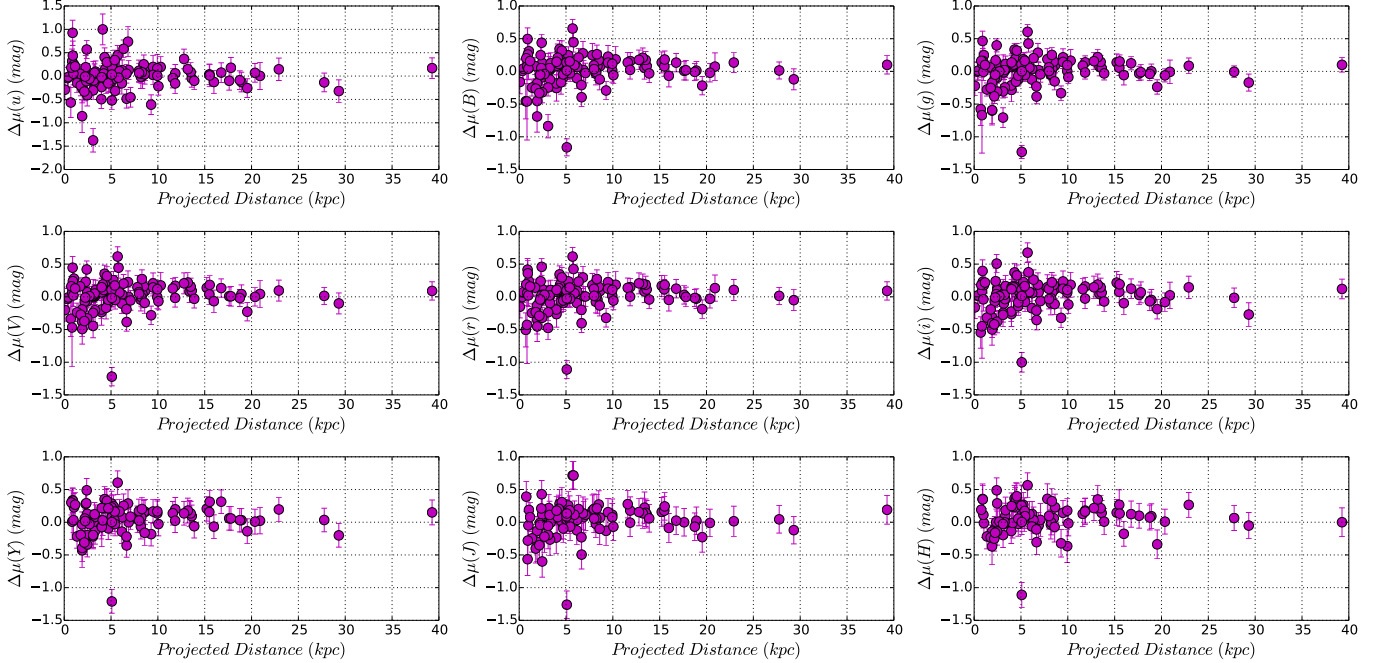


Figure 14. Variation of $\Delta\mu$ with projected distance from host centers in $uBgVriYJH$ bands. In all cases $\Delta\mu$ have smaller dispersion when they explode farther from their host centers.

SNe Ia from the Nearby Supernova Factory program and found a Δ_{HR} of -0.085 ± 0.028 mag, and a slope of -0.043 ± 0.014 mag dex $^{-1}$. Similar and consistent results were also presented from the SDSS (Lampeitl et al. 2010) and SNLS (Sullivan et al. 2010) samples. Uddin et al. (2017b) combined both spectroscopically confirmed and photometrically classified SNe Ia from multiple surveys and undertook a consistent analysis. They found a Δ_{HR} of -0.05 ± 0.01 mag from a sample of 1338 SNe Ia. In the CSP-I sample, we find similar correlations between Hubble residuals and host stellar mass across all wavelengths from optical to near-infrared, in apparent contradiction to the suggestion that dust explains the luminosity correction (Brout & Scolnic 2020).

- (b) Galbany et al. (2012) found no correlation (-0.0019 ± 0.0022 mag kpc $^{-1}$) between SN Ia Hubble residual and projected distance. The study presented in Hicken et al. (2009) is closer to this work, where they found 0.05 mag less dispersion in SNe Ia exploding beyond 12 kpc from their host centers.

Why do SNe Ia have larger Hubble residuals when they explode closer to their hosts, while the dispersion gets smaller when they explode farther away? We suspect that dust in host galaxies may play a role here, particularly since the difference in dis-

persion is largest at bluer wavelengths after eliminating the nearest SNe Ia. We examine this in Fig 15, where we encode $E(B - V)_{\text{host}}$ information in the plot of Hubble residual vs. projected distance. We see that SNe Ia that explode beyond 10 kpc from host centers have a smaller variation in $E(B - V)_{\text{host}}$. On the other hand, SNe Ia that explode within 10 kpc of host centers have a large variation of $E(B - V)_{\text{host}}$. Moreover, it seems that SNe Ia with higher color excess are also more luminous after light-curve standardization (negative values of Hubble residuals).

In Fig. 16, we plot both $E(B - V)_{\text{host}}$ and the extinction law R_V^{host} with respect to the projected distance. One can see that SNe Ia that explode within 10 kpc of their host centers have large variations in color excess, whereas those that explode beyond 10 kpc of their host center have smaller variations in color excess. The extinction law seems not to vary according to separation.

- (c) Hicken et al. (2009) found that SNe Ia in spiral galaxies (Scd/Sd/Irr) are intrinsically fainter than their E/S0 counterparts by 0.14 ± 0.07 mag, after light-curve correction. We have used galaxy morphological information in subsection 4.1, and use it again to examine how SN Ia Hubble residuals are distributed when they are grouped according to host morphological types. We do not find a sig-

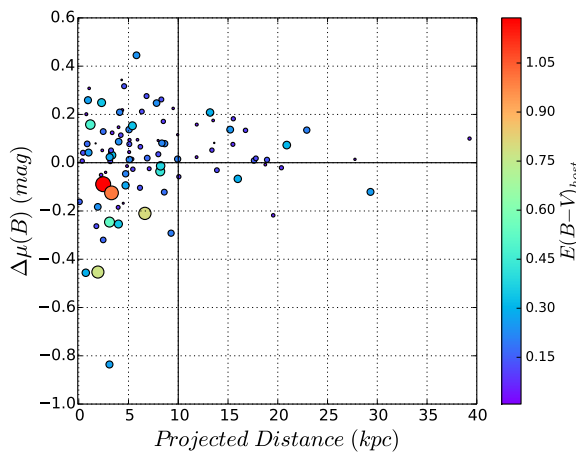


Figure 15. Plot of SN Ia B -band Hubble residual vs. projected distances from host centers. Symbols in this dispersion plot are varying according to respective color excess values, $E(B-V)_{\text{host}}$. Redder and larger symbols refer to higher color excess. SNe Ia with larger color excess tend to reside closer to hosts and are more luminous.

nificant difference in the weighted means of $\Delta\mu(B)$ between spiral hosts and E/S0 hosts as we measure a difference of 0.02 ± 0.09 mag in $\Delta\mu(B)$ between them. We summarize the weighted means in Table 4. A recent study by Prughinskaya et al. (2020) also supports our findings where they did not observe any difference in $\Delta\mu(B)$ between Early-type and Late-type SN Ia host galaxies.

We note that galaxy morphology from NED is not homogeneous. The morphological classification method and images that are used to classify galaxies are also variable. A consistent classification scheme is therefore preferable.

Table 4. Weighted mean of SN Ia Hubble residual in different host morphological types.

Morphology	No.	Weighted mean of $\Delta\mu(B)$ (mag)
Spiral	59	0.026 ± 0.051
E	9	-0.038 ± 0.137
S0	21	0.056 ± 0.087
E +S0	30	0.028 ± 0.074

6. CONCLUSION

We have presented photometry of host galaxies of SNe Ia from the CSP-I in $ugriYJH$ filters. We have determined host galaxy stellar masses, and have studied the corre-

lation between host galaxy stellar mass and SNe Ia Hubble residual in the $uBgVriYJH$ bands. We emphasize that this is the first time such a study has been made using optical and near-infrared Hubble residuals of SNe Ia. Our results are consistent with previous studies that SNe Ia are on average more luminous in massive hosts, after correcting for the luminosity-decline rate relation. Moreover, we find that the Hubble residual offset, Δ_{HR} , is approximately constant from optical to near-infrared wavelengths, suggesting that dust in SNe Ia host galaxies does not play a large role in driving these correlations. We have also determined projected distances between the SNe and the centers of their host galaxies. We find that SNe Ia that explode beyond 10 kpc from their host galaxy centers have a smaller dispersion in their luminosities compared to those that explode within 10 kpc. These SNe also have a smaller variation in color excess than do SNe that explode within 10 kpc. SNe Ia exploding closer to host centers also more commonly have higher color excesses. These results should be confirmed with a larger sample with host galaxies clearly identified. We did not find differences in SN Ia standardized luminosities when they are grouped according to their host morphological types.

We are gathering integral-field spectroscopy of CSP SN Ia host galaxies (e.g., Galbany et al. 2018) to study their local environments. This may provide more insight into the origin of the observed luminosity offsets along with other findings.

ACKNOWLEDGMENTS

We thank the anonymous referee for helping to improve this paper. The work of the *Carnegie Supernova Project* has been supported by the National Science Foundation under grants AST0306969, AST0607438, AST1008343, AST1613426, AST1613472, and AST613455. NBS and KK gratefully acknowledge the support from the George P. and Cynthia Woods Mitchell Institute for Fundamental Physics and Astronomy. We also thank the Mitchell Foundation for their support of the Cooks Branch Workshop on Supernovae. M. S. is funded by generous grants from the Villum FONDEN No. 24349 and the Independent Research Fund Denmark No. 29774. L.G. was funded by the European Union’s Horizon 2020 research and innovation program under the Marie Skłodowska-Curie grant agreement No. 839090. This work has been partially supported by the Spanish grant PGC2018-095317-B-C21 within the European Funds for Regional Development (FEDER).

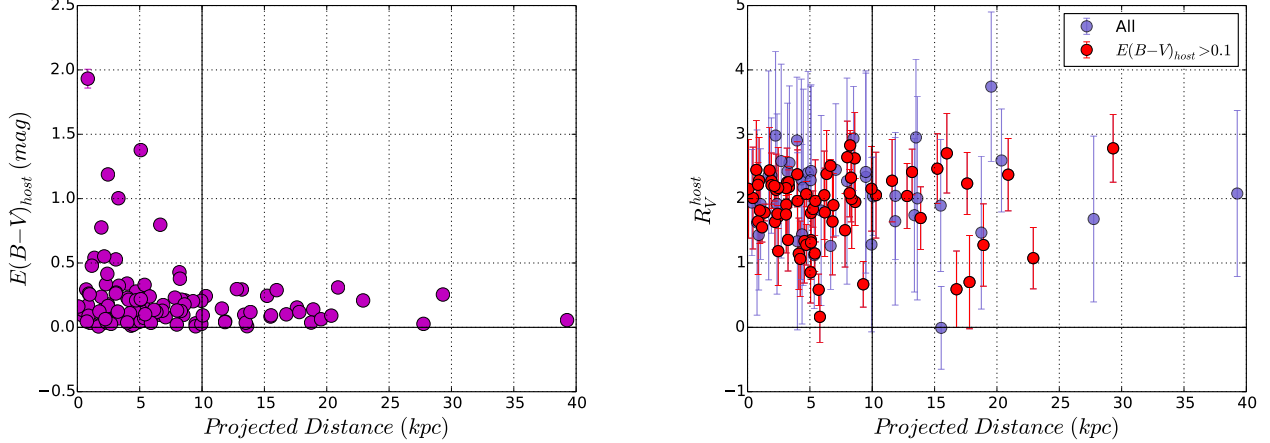


Figure 16. *Left:* Variation of color excess $E(B-V)_{\text{host}}$, and extinction law R_V^{host} , at the position of SN Ia as a function of the projected distance. On average, SNe Ia exploding beyond 10 kpc have $E(B-V)_{\text{host}} < 0.5$ mag. The largest color excess is observed for SN 2008cd, which is within 5.5 arcseconds from its host NGC 5038. *Right:* Variation of extinction law R_V^{host} at the position of SNe Ia as a function of the projected distance. We do not observe significant variation of R_V^{host} .

APPENDIX

A. SN IA HUBBLE RESIDUAL

We include multi-band Hubble residual for each SN Ia used in this work.

Table A1. CSP-I SN Ia Hubble Residuals

<i>SN Name</i>	z_{CMB}	<i>u</i>	<i>B</i>	<i>g</i>	<i>V</i>	<i>r</i>	<i>i</i>	<i>Y</i>	<i>J</i>	<i>H</i>
2004ef	0.031	0.13(0.20)	0.02(0.15)	0.02(0.12)	-0.00(0.15)	0.01(0.15)	0.07(0.16)	-0.00(0.20)	0.08(0.24)	-0.05(0.20)
2004eo	0.016	-0.13(0.21)	0.01(0.14)	0.00(0.11)	0.04(0.14)	-0.03(0.15)	-0.05(0.16)	0.03(0.18)	0.02(0.21)	0.09(0.19)
2004ey	0.016	0.15(0.23)	0.22(0.14)	0.19(0.11)	0.22(0.14)	0.19(0.14)	0.16(0.15)	0.24(0.18)	0.17(0.21)	0.34(0.19)
2004gs	0.027	0.11(0.20)	0.08(0.14)	0.09(0.11)	0.09(0.14)	0.09(0.14)	0.12(0.15)	0.16(0.19)	0.07(0.23)	0.23(0.20)
2004gu	0.046	0.05(0.22)	0.13(0.16)	0.12(0.13)	0.07(0.16)	0.12(0.16)	0.13(0.16)	0.12(0.19)	0.12(0.29)	0.29(0.22)
2005A	0.019	...	-0.09(0.16)	-0.10(0.14)	-0.07(0.16)	0.03(0.16)	0.10(0.16)	-0.20(0.21)	-0.05(0.24)	-0.04(0.21)
2005ag	0.079	...	0.05(0.17)	0.07(0.14)	0.08(0.17)	0.08(0.17)	0.04(0.17)	0.13(0.20)	0.22(0.24)	...
2005al	0.012	0.40(0.20)	0.34(0.13)	0.33(0.09)	0.35(0.13)	0.34(0.13)	0.37(0.14)	0.35(0.19)	0.28(0.22)	0.36(0.20)
2005am	0.008	-0.48(0.20)	-0.40(0.14)	-0.39(0.11)	-0.39(0.14)	-0.41(0.14)	-0.35(0.15)	-0.35(0.18)	-0.49(0.22)	-0.30(0.19)
2005be	0.035	-0.09(0.24)	-0.01(0.17)	-0.03(0.14)	-0.04(0.16)	-0.01(0.15)	-0.01(0.16)
2005bg	0.023	-0.04(0.23)	0.01(0.17)	-0.00(0.14)	-0.03(0.16)	-0.00(0.16)	0.02(0.17)
2005bl	0.024	0.00(0.27)	0.08(0.22)	0.04(0.20)	0.04(0.21)	-0.04(0.22)	0.07(0.20)
2005bo	0.014	-0.23(0.23)	-0.25(0.20)	-0.28(0.18)	-0.23(0.20)	-0.26(0.20)	-0.26(0.19)
2005el	0.015	-0.05(0.19)	0.08(0.13)	0.05(0.09)	0.09(0.13)	0.11(0.13)	0.06(0.14)	0.09(0.17)	0.12(0.21)	0.14(0.19)
2005eq	0.029	-0.10(0.20)	0.01(0.14)	-0.03(0.11)	0.01(0.14)	0.03(0.14)	0.03(0.15)	0.06(0.18)	-0.00(0.21)	0.10(0.19)
2005hc	0.046	0.25(0.20)	0.17(0.14)	0.15(0.11)	0.16(0.14)	0.15(0.14)	0.18(0.15)	0.15(0.18)	0.27(0.21)	0.06(0.21)
2005hj	0.058	-0.13(0.25)	0.05(0.18)	0.03(0.15)	-0.00(0.17)	-0.00(0.17)	0.06(0.17)	-0.02(0.20)	0.02(0.25)	...
2005iq	0.034	0.09(0.20)	0.17(0.13)	0.14(0.10)	0.15(0.13)	0.18(0.13)	0.14(0.14)	0.14(0.18)	0.14(0.21)	0.21(0.19)
2005ir	0.076	-0.02(0.21)	0.04(0.16)	0.01(0.14)	-0.01(0.16)	0.07(0.16)	0.02(0.16)
2005kc	0.015	-0.06(0.20)	0.03(0.14)	0.02(0.11)	0.02(0.14)	0.03(0.14)	-0.04(0.15)	-0.02(0.18)	0.00(0.21)	0.10(0.19)
2005ke	0.005	0.45(0.21)	0.66(0.14)	0.60(0.11)	0.61(0.15)	0.61(0.14)	0.68(0.15)	0.60(0.18)	0.71(0.21)	0.56(0.19)
2005ki	0.019	-0.14(0.20)	0.01(0.13)	-0.01(0.09)	0.01(0.13)	0.01(0.13)	-0.02(0.15)	0.03(0.18)	0.04(0.21)	0.06(0.19)
2005ku	0.045	0.32(0.26)	0.08(0.20)	0.12(0.18)	0.06(0.20)	0.06(0.19)	0.09(0.19)	0.01(0.27)
2005lu	0.032	0.19(0.25)	0.25(0.21)	0.17(0.18)	0.23(0.21)	0.24(0.21)	0.24(0.20)	0.28(0.21)
2005M	0.022	-0.09(0.20)	0.01(0.14)	-0.01(0.11)	0.02(0.14)	-0.00(0.14)	-0.10(0.15)	0.01(0.18)	0.22(0.21)	-0.02(0.19)
2005mc	0.025	0.03(0.28)	0.02(0.25)	0.02(0.23)	0.02(0.24)	0.01(0.23)	0.04(0.22)
2005ma	0.026	-0.49(0.20)	-0.18(0.14)	-0.21(0.11)	-0.20(0.14)	-0.20(0.14)	-0.23(0.15)	-0.07(0.18)	-0.23(0.24)	-0.14(0.19)
2005W	0.009	0.19(0.22)	0.18(0.20)	0.16(0.17)	0.17(0.20)	0.18(0.20)	0.18(0.19)
2006ax	0.017	-0.09(0.20)	-0.01(0.13)	-0.04(0.10)	-0.02(0.13)	-0.02(0.13)	-0.07(0.14)	0.03(0.18)	-0.07(0.21)	0.07(0.19)
2006bd	0.026	...	0.25(0.18)	0.19(0.16)	0.15(0.18)	0.18(0.18)	0.15(0.19)	0.05(0.20)	0.18(0.24)	0.36(0.23)
2006bh	0.011	0.06(0.19)	0.16(0.13)	0.14(0.10)	0.17(0.13)	0.15(0.13)	0.16(0.14)	0.20(0.18)	0.18(0.21)	0.18(0.19)
2006br	0.025	...	-0.12(0.18)	-0.24(0.15)	-0.20(0.19)	-0.10(0.19)	-0.04(0.19)	-0.14(0.29)	-0.27(0.24)	-0.01(0.22)
2006D	0.009	-0.01(0.19)	-0.06(0.13)	-0.10(0.10)	-0.07(0.14)	-0.06(0.14)	-0.07(0.15)	0.06(0.18)	-0.01(0.22)	-0.10(0.19)
2006ef	0.018	0.20(0.25)	0.23(0.17)	0.21(0.13)	0.20(0.16)	0.23(0.15)
2006ej	0.021	0.09(0.23)	0.12(0.16)	0.11(0.12)	0.10(0.15)	0.10(0.15)	0.16(0.16)	0.08(0.18)	-0.01(0.22)	0.18(0.20)
2006eq	0.050	0.17(0.30)	0.01(0.18)	0.01(0.15)	-0.01(0.17)	0.01(0.17)	0.07(0.18)	0.14(0.19)	0.12(0.24)	-0.36(0.25)
2006et	0.022	-0.04(0.19)	-0.09(0.13)	-0.12(0.10)	-0.08(0.13)	-0.09(0.13)	-0.14(0.14)	-0.09(0.17)	-0.04(0.21)	-0.02(0.19)
2006ev	0.029	...	0.14(0.16)	0.14(0.13)	0.14(0.16)	0.17(0.16)	0.22(0.17)	0.21(0.19)	0.16(0.22)	0.15(0.20)
2006fw	0.083	-0.57(0.32)	-0.46(0.27)	-0.58(0.25)	-0.34(0.27)	-0.51(0.26)	-0.55(0.24)

Table A1 *continued*

Table A1 (*continued*)

<i>SN Name</i>	z_{CMB}	<i>u</i>	<i>B</i>	<i>g</i>	<i>V</i>	<i>r</i>	<i>i</i>	<i>Y</i>	<i>J</i>	<i>H</i>	<i>I</i>
2006gj	0.028	0.15(0.21)	0.2(0.15)	0.22(0.12)	0.22(0.15)	0.20(0.15)	0.19(0.16)	0.18(0.19)	0.14(0.23)	0.35(0.21)	
2006gt	0.045	0.04(0.22)	0.08(0.15)	0.06(0.12)	0.04(0.15)	0.12(0.15)	0.08(0.16)	0.16(0.18)	0.18(0.22)	0.27(0.23)	
2006hb	0.015	0.13(0.22)	0.07(0.15)	0.04(0.11)	0.04(0.15)	0.09(0.15)	0.06(0.16)	0.08(0.19)	0.04(0.22)	0.13(0.19)	
2006hx	0.045	-0.14(0.21)	-0.18(0.15)	-0.17(0.12)	-0.19(0.15)	-0.13(0.15)	-0.31(0.16)	-0.03(0.19)	-0.13(0.22)	-0.14(0.20)	
2006is	0.031	-0.08(0.29)	-0.17(0.18)	-0.16(0.16)	-0.17(0.17)	-0.07(0.17)	0.11(0.19)	0.28(0.22)	0.02(0.28)	0.34(0.26)	
2006kf	0.021	0.01(0.21)	0.09(0.15)	0.09(0.12)	0.11(0.15)	0.08(0.14)	0.10(0.15)	0.09(0.18)	0.10(0.21)	0.10(0.20)	
2006lu	0.053	-0.11(0.25)	0.04(0.17)	-0.01(0.14)	0.01(0.16)	0.03(0.16)	-0.01(0.17)	0.28(0.19)	
2006mr	0.006	-0.86(0.35)	-0.69(0.24)	-0.60(0.22)	-0.38(0.23)	-0.34(0.23)	-0.50(0.24)	-0.43(0.26)	-0.30(0.30)	-0.37(0.28)	
2006rb	0.059	-0.46(0.21)	-0.03(0.15)	-0.04(0.12)	0.06(0.15)	0.01(0.15)	-0.07(0.15)	0.09(0.20)	0.12(0.24)	0.04(0.25)	
2006es	0.033	-0.02(0.25)	-0.04(0.17)	-0.06(0.14)	-0.05(0.17)	-0.08(0.17)	-0.10(0.18)	-0.07(0.19)	-0.03(0.21)	-0.04(0.22)	
2006py	0.058	-0.29(0.22)	-0.16(0.18)	-0.22(0.15)	-0.20(0.17)	-0.15(0.17)	-0.16(0.17)	
2006X	0.005	-0.52(0.19)	-1.16(0.13)	-1.23(0.10)	-1.22(0.14)	-1.11(0.14)	-1.00(0.15)	-1.21(0.18)	-1.26(0.21)	-1.11(0.19)	
2007af	0.005	0.25(0.19)	0.25(0.13)	0.19(0.10)	0.26(0.13)	0.24(0.13)	0.23(0.14)	0.25(0.17)	0.26(0.21)	0.27(0.19)	
2007ai	0.032	-0.13(0.25)	-0.07(0.17)	-0.06(0.15)	-0.07(0.17)	-0.05(0.17)	-0.10(0.17)	-0.07(0.18)	-0.09(0.22)	-0.18(0.19)	
2007al	0.012	0.25(0.28)	0.31(0.19)	0.25(0.16)	0.28(0.18)	0.24(0.17)	0.18(0.19)	0.23(0.21)	0.19(0.25)	-0.01(0.22)	
2007as	0.018	0.20(0.21)	0.08(0.14)	0.06(0.11)	0.04(0.14)	0.03(0.14)	0.11(0.15)	0.08(0.18)	0.04(0.21)	0.12(0.19)	
2007ax	0.007	0.93(0.27)	0.49(0.17)	0.47(0.15)	0.45(0.17)	0.41(0.17)	0.40(0.17)	0.34(0.19)	-0.56(0.25)	0.35(0.23)	
2007ba	0.038	-0.61(0.21)	-0.29(0.14)	-0.33(0.11)	-0.28(0.14)	-0.32(0.14)	-0.32(0.15)	-0.18(0.18)	-0.13(0.22)	-0.32(0.21)	
2007bc	0.021	-0.10(0.19)	-0.03(0.14)	-0.03(0.10)	-0.03(0.14)	-0.04(0.14)	-0.07(0.15)	-0.06(0.18)	0.06(0.21)	0.01(0.20)	
2007bd	0.031	-0.06(0.21)	0.01(0.13)	-0.03(0.10)	0.01(0.14)	-0.01(0.14)	0.01(0.15)	0.04(0.18)	0.04(0.22)	0.06(0.20)	
2007bm	0.006	-0.15(0.20)	-0.25(0.13)	-0.28(0.10)	-0.24(0.14)	-0.25(0.14)	-0.32(0.15)	-0.22(0.18)	-0.25(0.21)	-0.22(0.19)	
2007ca	0.014	0.05(0.20)	-0.01(0.13)	-0.04(0.10)	0.00(0.14)	0.01(0.14)	-0.02(0.15)	0.08(0.18)	0.06(0.21)	-0.00(0.19)	
2007cg	0.033	-0.26(0.31)	-0.45(0.23)	-0.59(0.20)	-0.49(0.23)	-0.45(0.23)	-0.40(0.22)	-0.39(0.21)	
2007hj	0.014	0.30(0.21)	0.32(0.15)	0.32(0.11)	0.32(0.15)	0.30(0.15)	0.33(0.16)	0.33(0.19)	0.31(0.22)	0.40(0.20)	
2007hx	0.080	0.00(0.29)	0.07(0.21)	-0.01(0.18)	0.04(0.21)	0.13(0.20)	0.02(0.20)	0.02(0.20)	
2007jd	0.073	0.74(0.32)	0.28(0.18)	0.29(0.14)	0.23(0.17)	0.30(0.17)	0.19(0.18)	0.29(0.21)	0.14(0.25)	...	
2007jg	0.037	0.58(0.19)	0.21(0.14)	0.20(0.11)	0.20(0.14)	0.23(0.14)	0.26(0.15)	0.25(0.18)	0.20(0.21)	0.03(0.20)	
2007jh	0.041	...	0.09(0.22)	0.07(0.20)	0.07(0.21)	0.08(0.21)	0.15(0.20)	-0.07(0.30)	
2007je	0.007	0.57(0.19)	0.44(0.13)	0.40(0.10)	0.42(0.13)	0.46(0.13)	0.51(0.14)	0.49(0.18)	0.43(0.21)	0.49(0.19)	
2007N	0.013	1.00(0.33)	0.21(0.21)	0.09(0.18)	0.19(0.21)	0.10(0.21)	0.16(0.21)	0.03(0.23)	0.08(0.26)	-0.01(0.23)	
2007jq	0.045	-0.26(0.20)	-0.22(0.14)	-0.24(0.11)	-0.23(0.14)	-0.19(0.14)	-0.19(0.15)	-0.14(0.19)	-0.23(0.23)	-0.34(0.22)	
2007jl	0.056	0.05(0.20)	0.08(0.13)	0.06(0.10)	0.16(0.13)	0.14(0.13)	0.12(0.13)	0.12(0.14)	0.16(0.18)	0.15(0.21)	0.14(0.19)
2007jn	0.006	0.02(0.20)	0.13(0.13)	0.14(0.10)	0.14(0.13)	0.12(0.13)	0.12(0.14)	-0.25(0.14)	-0.22(0.17)	-0.20(0.21)	-0.20(0.19)
2007js	0.014	-0.31(0.19)	-0.25(0.13)	-0.31(0.10)	-0.25(0.13)	-0.24(0.13)	-0.24(0.13)	-0.32(0.16)	-0.38(0.17)	-0.34(0.19)	-0.14(0.21)
2007jt	0.021	-0.41(0.23)	-0.32(0.16)	-0.31(0.13)	-0.33(0.16)	-0.33(0.16)	-0.32(0.16)	-0.32(0.16)	-0.34(0.19)	-0.30(0.24)	-0.20(0.19)
2007jx	0.031	0.05(0.21)	0.11(0.14)	0.10(0.11)	0.10(0.14)	0.13(0.14)	0.14(0.15)	0.21(0.18)	0.20(0.21)	0.23(0.19)	
2008er	0.026	0.07(0.19)	0.05(0.13)	0.02(0.10)	0.05(0.14)	0.02(0.14)	0.03(0.15)	0.12(0.18)	0.11(0.21)	0.00(0.19)	
2008bc	0.015	0.10(0.24)	0.10(0.14)	0.06(0.11)	0.07(0.14)	0.06(0.14)	0.07(0.15)	0.17(0.18)	0.12(0.21)	0.12(0.19)	
2008bi	0.013	0.44(0.31)	0.26(0.23)	0.16(0.19)	0.24(0.21)	0.36(0.20)	0.23(0.20)	0.38(0.19)	-0.28(0.25)	0.35(0.21)	
2008bq	0.034	0.04(0.21)	-0.12(0.16)	-0.15(0.13)	-0.09(0.16)	-0.13(0.16)	-0.11(0.16)	-0.16(0.19)	-0.10(0.24)	-0.07(0.23)	
2008bt	0.015	0.02(0.22)	0.14(0.16)	0.11(0.13)	0.11(0.16)	0.10(0.16)	0.11(0.17)	0.23(0.19)	0.09(0.26)	0.26(0.31)	

Table A1 *continued*

Table A1 (*continued*)

<i>SN Name</i>	z_{CMB}	<i>u</i>	<i>B</i>	<i>g</i>	<i>V</i>	<i>r</i>	<i>i</i>	<i>Y</i>	<i>J</i>	<i>H</i>
2008bz	0.060	0.11(0.23)	0.09(0.15)	0.06(0.12)	0.07(0.14)	0.12(0.16)	0.17(0.18)	0.20(0.23)
2008C	0.017	0.05(0.24)	0.04(0.17)	-0.01(0.13)	0.02(0.17)	-0.04(0.18)	0.03(0.19)	-0.05(0.23)	0.11(0.20)	0.11(0.20)
2008cc	0.010	-0.20(0.22)	-0.26(0.15)	-0.25(0.11)	-0.27(0.15)	-0.19(0.16)	-0.19(0.18)	-0.40(0.22)	-0.23(0.19)	-0.23(0.19)
2008cd	0.007	...	-0.46(0.59)	-0.67(0.58)	-0.47(0.60)	-0.43(0.59)	-0.45(0.49)
2008cf	0.046	-0.11(0.23)	0.05(0.15)	-0.01(0.12)	-0.01(0.15)	0.02(0.14)	0.04(0.16)	0.29(0.19)	0.21(0.27)	0.00(0.20)
2008fl	0.020	-0.15(0.23)	-0.10(0.16)	-0.12(0.12)	-0.10(0.15)	-0.09(0.15)	-0.17(0.17)	-0.14(0.18)	-0.12(0.22)	-0.06(0.20)
2008fp	0.006	-0.33(0.20)	-0.33(0.14)	-0.38(0.11)	-0.37(0.15)	-0.29(0.15)	-0.42(0.16)	-0.31(0.18)	-0.35(0.21)	-0.25(0.19)
2008fr	0.039	0.18(0.26)	0.20(0.15)	0.16(0.12)	0.16(0.15)	0.19(0.15)	0.18(0.16)	0.30(0.19)	0.39(0.23)	0.19(0.19)
2008fu	0.052	-0.06(0.22)	-0.04(0.16)	-0.00(0.12)	0.01(0.15)	0.03(0.14)	0.01(0.16)	-0.03(0.19)	-0.22(0.24)	0.01(0.20)
2008fw	0.009	-0.04(0.21)	0.14(0.15)	0.09(0.11)	0.13(0.15)	0.14(0.15)	0.12(0.16)	0.14(0.18)	0.28(0.21)	0.13(0.19)
2008gs	0.032	0.14(0.24)	0.14(0.15)	0.09(0.12)	0.10(0.16)	0.10(0.16)	0.14(0.17)	0.20(0.18)	0.01(0.23)	0.27(0.19)
2008l	0.034	0.07(0.21)	0.13(0.14)	0.12(0.10)	0.13(0.14)	0.12(0.14)	0.12(0.15)	0.31(0.18)	0.02(0.21)	0.12(0.20)
2008so	0.062	0.18(0.22)	0.02(0.15)	-0.01(0.12)	0.01(0.15)	-0.00(0.15)	0.07(0.16)	0.06(0.18)
2008sp	0.033	-0.16(0.22)	0.02(0.14)	-0.02(0.10)	-0.02(0.14)	0.00(0.14)	-0.03(0.15)	0.02(0.18)	-0.01(0.21)	0.16(0.20)
2008tij	0.038	0.01(0.24)	0.18(0.13)	0.15(0.10)	0.18(0.14)	0.18(0.14)	0.19(0.15)	0.31(0.17)	0.24(0.21)	0.13(0.20)
2008uu	0.050	0.17(0.22)	0.10(0.14)	0.10(0.11)	0.09(0.14)	0.09(0.14)	0.12(0.15)	0.15(0.19)	0.19(0.22)	0.00(0.22)
2008uv	0.013	0.01(0.20)	0.12(0.13)	0.10(0.09)	0.12(0.13)	0.11(0.13)	0.11(0.14)	0.17(0.18)	0.08(0.21)	0.18(0.19)
2008ia	0.022	-0.01(0.21)	-0.05(0.15)	-0.05(0.12)	-0.01(0.15)	-0.04(0.15)	-0.01(0.15)	0.02(0.18)	-0.04(0.21)	-0.16(0.19)
2008O	0.039	0.34(0.21)	0.15(0.15)	0.16(0.12)	0.17(0.15)	0.14(0.15)	0.16(0.16)	0.16(0.18)	0.18(0.22)	0.17(0.20)
2008R	0.013	-0.02(0.24)	0.15(0.14)	0.14(0.11)	0.15(0.14)	0.11(0.14)	0.12(0.15)	0.22(0.19)	0.18(0.22)	0.25(0.20)
2009aa	0.027	-0.22(0.19)	-0.06(0.13)	-0.09(0.10)	-0.07(0.13)	-0.06(0.14)	-0.12(0.14)	-0.03(0.18)	-0.07(0.21)	-0.02(0.19)
2009ab	0.011	0.08(0.20)	0.26(0.14)	0.25(0.11)	0.27(0.14)	0.27(0.14)	0.22(0.15)	0.20(0.18)	0.21(0.21)	0.32(0.19)
2009ad	0.028	-0.32(0.20)	-0.03(0.13)	-0.06(0.10)	-0.05(0.14)	-0.03(0.14)	-0.08(0.15)	-0.03(0.18)	-0.07(0.21)	0.09(0.19)
2009ag	0.009	0.37(0.21)	0.18(0.15)	0.16(0.13)	0.21(0.16)	0.21(0.16)	0.15(0.17)	0.14(0.18)	0.16(0.21)	0.22(0.19)
2009al	0.022	-0.32(0.24)	-0.12(0.16)	-0.17(0.13)	-0.10(0.16)	-0.05(0.16)	-0.27(0.18)	-0.20(0.18)	-0.12(0.21)	-0.05(0.20)
2009cz	0.021	0.07(0.20)	0.04(0.13)	0.01(0.11)	0.04(0.14)	0.01(0.14)	-0.04(0.15)	0.03(0.18)	0.06(0.21)	0.10(0.20)
2009D	0.025	0.07(0.20)	-0.02(0.14)	-0.06(0.10)	-0.00(0.14)	-0.03(0.14)	-0.08(0.14)	0.01(0.19)	-0.01(0.21)	0.01(0.19)
2009ds	0.019	-0.16(0.20)	-0.05(0.14)	-0.07(0.10)	-0.05(0.14)	-0.06(0.14)	-0.09(0.15)	0.21(0.19)	-0.10(0.21)	0.05(0.19)
2009F	0.013	-1.38(0.25)	-0.84(0.18)	-0.71(0.15)	-0.45(0.18)	-0.48(0.18)	-0.28(0.18)	-0.20(0.21)	-0.06(0.24)	-0.03(0.22)
2009I	0.026	0.05(0.20)	-0.21(0.14)	-0.23(0.10)	-0.19(0.14)	-0.20(0.14)	-0.21(0.15)	-0.22(0.18)	-0.23(0.21)	-0.11(0.19)
2009le	0.018	-0.04(0.23)	0.45(0.15)	0.42(0.13)	0.45(0.16)	0.42(0.16)	0.38(0.16)	...	0.71(0.21)	...
2009P	0.025	0.21(0.20)	0.16(0.16)	0.10(0.13)	0.13(0.16)	0.16(0.16)	0.22(0.16)	0.27(0.19)	0.08(0.22)	...
2009Y	0.009	0.03(0.20)	0.01(0.14)	0.00(0.11)	-0.02(0.14)	-0.03(0.14)	0.01(0.15)	0.00(0.18)	0.13(0.21)	0.00(0.19)

B. HOST GALAXY PHOTOMETRY

We include a table of $ugriYJH$ photometry of CSP-I SN Ia host galaxies. Values within parentheses are uncertainties of measurements. When photometry is not available, it is shown as \dots . Morphological classifications are taken from the NED.

Table B1. CSP-I Host Galaxy Photometry

<i>SN Name</i>	<i>Host Galaxy Name</i>	Morphology	<i>u</i>	<i>g</i>	<i>r</i>	<i>i</i>	<i>Y</i>	<i>J</i>	<i>H</i>
2004ef	UGC 12158	SA	17.44(08)	14.07(04)	13.40(06)	13.12(03)	12.39(12)	11.77(12)	11.12(09)
2004eo	NGC 6928	SB	14.64(08)	12.68(05)	11.83(08)	11.09(13)	...	9.81(02)	9.07(03)
2004ey	UGC 11816	SB	18.02(08)	13.90(06)	13.44(11)	13.18(11)	12.08(05)	12.23(06)	11.54(08)
2004gs	MCG +03-22-020	S	16.65(08)	14.65(06)	13.72(11)	13.32(11)	12.46(10)	12.05(09)	11.33(09)
2004gu	FGC 175A	...	19.24(09)	17.23(08)	16.48(08)	16.01(08)	14.53(09)	14.07(10)	13.16(12)
2005A	NGC 958	SB	14.29(09)	12.49(11)	11.85(09)	11.41(12)	10.49(12)	9.91(14)	9.03(16)
2005ag	2MASS J14564320+0919366	16.26(08)	15.49(07)	15.06(08)	14.14(07)	13.57(12)	12.97(10)
2005al	NGC 5304	cD	15.17(10)	13.22(07)	12.37(06)	11.99(07)	10.93(16)	10.14(14)	9.94(12)
2005am	NGC 2811	SB	13.55(09)	11.70(09)	10.93(09)	10.50(09)	9.32(09)	8.90(08)	8.38(08)
2005be	2MASS J14593308+1640068	...	17.67(07)	15.45(11)	14.51(11)	14.16(06)	...	12.76(04)	12.01(05)
2005bg	MCG +03-31-93	...	15.89(14)	14.79(12)	14.24(14)	14.02(13)	...	12.96(04)	12.33(06)
2005bl	NGC 4059	E	15.55(14)	13.48(11)	12.68(09)	12.20(06)	...	10.73(02)	10.01(02)
2005bo	NGC 4708	SA	16.03(07)	13.79(10)	13.10(10)	12.40(04)	...	11.16(03)	10.52(04)
2005el	NGC 1819	S0	15.38(10)	13.37(06)	12.17(09)	11.79(07)	10.89(09)	10.44(10)	9.78(10)
2005eq	MCG -01-09-006	SB	17.00(09)	14.18(03)	13.53(08)	13.16(10)	12.75(14)	12.36(15)	11.75(16)
2005hc	MCG +00-06-003	...	18.50(11)	15.66(08)	14.91(10)	14.54(10)	13.59(13)	13.21(20)	12.55(12)
2005hj	APMUKS(BJ) B012415.21-012950.3	...	20.05(12)	18.99(02)	18.26(01)	17.88(02)	16.81(10)	16.24(11)	15.43(28)
2005iq	MCG -03-01-008	SA	17.76(09)	15.01(08)	14.29(09)	13.94(08)	13.08(12)	12.60(18)	12.07(19)
2005ir	SDSS J011643.87+004736.9	...	18.58(04)	17.40(08)	16.87(07)	16.49(06)	...	15.77(14)	15.01(19)
2005kc	NGC 7311	SA	14.25(15)	12.50(05)	11.76(07)	11.33(07)	10.40(09)	9.22(07)	8.67(09)
2005ke	NGC 1371	SA	14.85(13)	11.74(05)	10.84(09)	10.43(03)	...	8.75(02)	8.08(02)
2005ki	NGC 3332	SA	15.33(07)	13.37(07)	12.53(02)	12.11(01)	11.15(11)	10.61(17)	10.07(10)
2005ku	2MASX J22594265-0000478	...	17.76(14)	16.41(09)	15.87(06)	15.66(09)	14.72(11)	14.31(10)	13.82(11)
2005lu	ESO 545-G038	S0	16.26(14)	15.49(04)	14.55(29)	14.28(07)	...	13.19(04)	12.44(06)
2005M	NGC 2930	S0	15.20(20)	14.32(08)	14.02(14)	13.98(12)	13.45(14)	14.45(15)	12.37(12)
2005mc	UGC 4414	SB	16.84(37)	14.70(05)	13.47(09)	12.86(10)	...	11.55(02)	10.80(03)
2005ma	UGC 3634	SB	16.14(07)	13.87(04)	12.93(04)	12.53(06)	11.71(12)	11.23(15)	10.47(14)
2005W	NGC 691	SA	15.64(11)	12.93(09)	12.05(13)	11.76(11)	...	9.68(02)	8.99(02)
2006ax	NGC 3663	SA	15.47(12)	14.06(04)	13.09(04)	12.14(04)	12.14(12)	11.38(12)	10.79(12)
2006bd	UGC 6609	E	17.52(32)	14.17(07)	13.34(05)	12.90(05)	11.71(12)	11.65(13)	10.98(17)
2006bh	NGC 7329	SB	15.56(16)	12.32(04)	11.68(06)	11.31(04)	10.88(07)	10.37(12)	9.86(07)
2006br	NGC 5185	S	16.04(05)	13.66(07)	12.99(05)	12.27(05)	11.59(09)	11.15(07)	10.45(12)
2006D	MCG -01-33-34	SB	15.64(10)	13.67(06)	13.08(05)	12.80(06)	12.09(08)	11.67(12)	10.98(11)
2006ef	NGC 809	S0	16.21(12)	13.96(06)	13.17(07)	12.77(06)	...	11.41(02)	10.72(02)
2006ej	NGC 191A	S0	16.55(22)	14.26(08)	13.42(06)	12.95(06)	11.92(09)	11.38(06)	10.72(08)
2006eq	2MASX J121238758+0113490	...	18.82(05)	17.33(07)	16.52(07)	16.07(07)	14.54(09)	14.23(09)	13.67(09)
2006et	NGC 232	SB	17.21(18)	14.05(06)	13.18(09)	12.73(07)	11.52(09)	11.19(06)	10.41(07)
2006ev	UGC 11758	S0	17.17(13)	14.35(02)	13.53(02)	13.10(03)	11.92(08)	11.37(06)	10.71(09)

Table B1 *continued*

Table B1 (*continued*)

<i>SN Name</i>	<i>Host Galaxy Name</i>	Morphology	<i>u</i>	<i>g</i>	<i>r</i>	<i>i</i>	<i>Y</i>	<i>J</i>	<i>H</i>
2006fw	SDSS J014710.33-000848.7	SA	19.85(23)	18.88(07)	18.28(08)	17.84(08)	...	16.68(12)	16.04(15)
2006gj	UGC 2650	SA	17.27(22)	14.98(04)	14.13(03)	13.69(04)	12.48(17)	12.03(13)	11.34(17)
2006gt	2MASX J00561810-0137327	...	19.72(28)	17.10(08)	16.26(06)	15.89(05)	15.21(13)	14.80(08)	14.14(14)
2006hb	MCG -04-12-34	E	16.47(08)	14.06(06)	13.08(03)	12.70(03)	11.94(08)	11.84(07)	11.47(08)
2006hx	2MASX J01135716+0022171	S0	18.49(09)	16.45(04)	15.70(04)	15.32(05)	14.17(07)	13.55(07)	12.91(09)
2006is	APMUKS(BJ) B051529.79-235009.8	19.25(14)	19.02(06)	18.98(07)	18.74(04)	19.73(05)	...
2006kf	UGC 2829	S0	16.57(08)	13.74(06)	12.93(04)	12.55(05)	11.38(09)	10.90(09)	10.33(11)
2006lu	2MASX J09151727-2536001	...	18.30(06)	16.29(05)	15.72(05)	15.39(05)	14.48(14)	14.04(07)	13.36(13)
2006mr	NGC 1316	S0	11.77(12)	9.84(05)	9.17(04)	8.66(03)	8.00(05)	6.80(05)	6.22(04)
2006ob	UGC 1333	SA	17.11(04)	15.18(07)	14.29(07)	13.86(07)	12.59(12)	11.93(11)	11.57(22)
2006os	UGC 2384	S	17.04(33)	14.43(04)	13.60(04)	13.24(04)	12.20(08)	11.66(09)	11.25(09)
2006py	SDSS J224142.04-000812.9	...	20.06(08)	18.23(07)	17.47(05)	17.05(04)	...	16.16(10)	15.50(12)
2006X	NGC 4321	SB	12.00(05)	11.00(05)	10.00(05)	9.90(05)	10.60(37)	9.76(12)	9.10(14)
2007af	NGC 5584	SB	14.92(03)	13.77(07)	13.11(07)	12.72(07)	11.74(10)	11.59(12)	11.07(10)
2007ai	MCG -04-38-004	SA	...	13.75(06)	12.84(02)	12.86(03)	12.05(09)	11.31(19)	10.72(11)
2007al	2MASX J09591870-1928233	...	17.95(09)	16.11(12)	15.03(05)	14.58(04)	13.59(11)	13.16(13)	12.62(07)
2007as	ESO 18-G18	SA	16.17(13)	13.61(13)	13.18(04)	12.86(12)	12.10(08)	11.62(09)	11.08(08)
2007ax	NGC 2577	S0	15.32(11)	12.79(04)	11.96(04)	11.53(04)	10.62(16)	10.01(11)	9.39(15)
2007ba	UGC 9798	S0	17.13(10)	14.13(07)	13.51(08)	13.06(07)	12.20(14)	11.85(15)	11.22(08)
2007bc	UGC 6332	SB	16.09(12)	13.64(10)	12.57(32)	12.50(05)	11.50(22)	11.23(17)	10.56(12)
2007bd	UGC 4455	SB	19.25(06)	14.41(06)	13.71(06)	13.35(07)	12.30(08)	11.80(08)	11.07(07)
2007bm	NGC 3672	SA	13.77(04)	11.84(11)	11.15(08)	10.75(06)	10.27(09)	9.73(06)	9.09(11)
2007ca	MCG -02-34-61	SA	18.71(24)	14.45(05)	13.96(06)	13.73(05)	12.90(16)	12.61(18)	11.84(10)
2007cg	ESO 508-G75	SA	17.28(09)	15.39(02)	14.65(02)	14.22(02)	13.23(07)	12.73(09)	12.06(10)
2007hj	NGC 7461	S0	16.41(11)	13.97(08)	13.11(05)	12.63(07)	11.57(02)	11.05(02)	10.52(02)
2007hx	SDSS J020627.93-005353.0	...	19.29(08)	16.96(06)	16.29(06)	15.82(05)	15.04(09)	14.27(07)	13.71(09)
2007jd	SDSS J025953.65+010936.1	...	18.75(13)	17.35(07)	16.77(08)	16.48(06)	15.61(16)	15.18(18)	14.20(16)
2007jg	SDSS J032950.83+003116.0	...	19.47(10)	18.74(08)	17.46(06)	17.49(07)	16.97(13)	17.27(17)	16.44(20)
2007jh	CGCG 391-014	E	17.22(08)	14.83(10)	13.85(20)	13.57(08)	12.50(13)	11.82(22)	11.29(16)
2007le	NGC 7721	SA	13.93(18)	12.35(04)	11.72(04)	11.39(05)	11.08(02)	10.38(09)	9.52(08)
2007N	MCG -01-33-012	SA	17.09(08)	14.03(09)	13.30(05)	12.96(07)	11.98(10)	11.42(10)	10.89(10)
2007nq	UGC 595	S	17.09(08)	14.53(10)	13.57(09)	13.10(09)	12.25(11)	11.81(12)	11.06(16)
2007ol	2MASX J01372378-0018422	...	18.96(15)	17.05(12)	16.29(12)	15.84(07)	...	14.62(13)	13.73(15)
2007on	NGC 1404	E	12.94(07)	10.72(11)	10.05(09)	9.59(08)	8.45(25)	8.23(25)	7.72(26)
2007S	UGC 3378	SA	15.43(18)	14.15(10)	13.74(08)	13.39(09)	12.51(06)	11.77(05)	11.48(08)
2007st	NGC 632	SB	14.62(07)	12.84(08)	12.14(13)	11.84(07)	11.06(09)	10.71(11)	9.90(20)
2007ux	2MASX J10091969+1459268	...	17.50(16)	15.76(05)	14.99(13)	14.59(16)	13.58(11)	13.09(15)	12.23(31)
2008ar	IC 3284	SA	17.05(16)	15.29(08)	14.64(11)	14.25(12)	13.14(24)	12.79(21)	12.33(23)
2008bc	KK 1524	...	16.18(06)	14.18(07)	13.16(11)	13.02(11)	12.43(14)	12.20(13)	11.20(15)
2008bi	NGC 2618	SA	16.37(06)	13.31(06)	12.53(09)	12.04(08)	10.36(53)	10.90(18)	10.40(07)
2008bq	ESO 308-G25	Sa	17.80(04)	14.19(01)	13.46(01)	13.06(01)	12.08(09)	11.61(09)	10.87(09)

Table B1 *continued*

Table B1 (*continued*)

<i>SN Name</i>	<i>Host Galaxy Name</i>	Morphology	<i>u</i>	<i>g</i>	<i>r</i>	<i>i</i>	<i>Y</i>	<i>J</i>	<i>H</i>
2008bt	NGC 3404	SB	15.43(09)	13.35(08)	12.46(08)	11.97(07)	10.76(09)	10.32(09)	9.67(09)
2008bz	2MASX J12385810+1107502	...	19.70(22)	16.55(06)	15.79(08)	15.34(09)	14.39(10)	13.93(14)	12.98(25)
2008C	UGC 3611	S0	16.33(14)	14.06(07)	13.31(09)	12.88(09)	11.96(12)	11.21(13)	10.58(13)
2008cc	ESO 107-G4	E	14.89(05)	12.79(06)	12.01(09)	11.62(08)	10.57(12)	10.15(17)	9.49(17)
2008cd	NGC 5038	S0	14.32(11)	12.78(03)	12.15(06)	11.81(05)	...	10.54(02)	9.83(01)
2008cf	LEDA 766647	...	19.09(07)	17.24(09)	16.64(07)	16.42(06)	16.87(20)	15.78(18)	15.37(20)
2008fj	NGC 6805	E	15.44(08)	13.26(02)	12.41(03)	11.97(04)	11.08(04)	10.59(08)	9.92(12)
2008fp	ESO 428-G14	S0	14.04(07)	12.42(06)	11.65(08)	11.05(06)	10.36(06)	9.83(07)	9.27(06)
2008fr	SDSS J011149.19+143826.5	...	20.83(14)	19.44(07)	18.77(11)	18.58(10)	18.72(15)	18.07(11)	17.76(12)
2008fu	ESO 480-IG-021	...	17.83(08)	15.57(09)	14.86(12)	14.49(11)	13.57(12)	13.07(11)	12.45(09)
2008fw	NGC 3261	SB	14.85(04)	12.66(09)	12.03(09)	11.41(10)	10.41(17)	10.03(16)	9.34(21)
2008gg	NGC 539	SB	16.48(06)	14.34(05)	13.53(15)	13.24(12)	12.59(09)	11.91(08)	11.51(08)
2008gl	UGC 881	E	16.78(18)	14.51(07)	13.68(12)	13.22(08)	12.35(15)	11.93(12)	11.19(24)
2008go	2MASX J22104396-2047256	...	18.08(10)	15.94(05)	14.98(07)	14.41(07)	13.72(14)	12.91(40)	11.68(64)
2008gp	MCG +00-9-74	SA	16.25(12)	14.20(09)	13.61(09)	13.26(08)	12.55(09)	12.03(11)	11.26(23)
2008hj	MCG -02-01-014	SB	16.76(03)	15.08(10)	14.37(05)	14.14(06)	13.84(08)	13.36(18)	12.52(11)
2008hu	ESO 561-G18	SA	17.77(07)	15.07(03)	14.06(03)	13.69(05)	13.06(06)	12.56(06)	11.49(07)
2008hv	NGC 2765	S0	14.83(01)	13.05(02)	12.28(02)	11.88(02)	10.79(07)	10.18(24)	9.70(11)
2008ia	ESO 125-6	S0	15.58(04)	13.17(11)	12.38(13)	12.02(13)	11.64(06)	10.86(16)	10.35(08)
2008O	ESO 256-G11	S0	16.10(06)	13.56(04)	12.79(03)	12.36(03)	11.19(02)	10.53(05)	9.85(05)
2008R	NGC 1200	S0	15.38(13)	13.04(28)	11.90(11)	11.41(10)	10.71(16)	10.23(20)	9.56(11)
2009aa	ESO 570-G20	Sc	19.91(14)	15.02(07)	14.42(00)	13.67(03)	13.15(09)	12.47(16)	12.04(17)
2009ab	UGC 2998	SB	16.90(16)	12.76(11)	12.22(13)	11.89(12)	11.25(18)	10.75(30)	10.01(44)
2009ad	UGC 3236	SA	16.97(10)	14.68(09)	13.98(11)	13.43(14)	12.69(08)	12.25(15)	11.61(10)
2009ag	ESO 492-2	SA	16.75(04)	12.02(11)	11.62(11)	11.37(12)	11.01(08)	10.52(08)	9.90(10)
2009al	NGC 3388	S0	16.14(03)	14.07(06)	13.35(07)	12.82(05)	11.81(07)	11.31(06)	10.64(09)
2009cz	NGC 2789	S0	15.01(16)	13.22(07)	12.61(07)	12.19(08)	11.56(17)	11.05(13)	10.36(15)
2009D	ESO 549-G031	SA	18.93(53)	14.31(14)	13.66(13)	13.32(12)	12.51(09)	12.01(11)	11.40(09)
2009ds	NGC 3905	SB	14.57(08)	13.37(10)	12.22(08)	11.15(12)	11.76(13)	10.99(13)	10.45(12)
2009F	NGC 1725	...	15.57(12)	13.23(08)	12.37(07)	11.67(11)	9.90(20)	9.96(25)	9.37(22)
2009I	NGC 1080	SA	15.26(07)	13.75(08)	12.93(06)	12.23(07)	12.09(08)	11.62(06)	11.10(08)
2009le	ESO 478-6	SA	13.99(08)	12.63(24)	12.08(06)	11.88(08)	10.96(22)	10.59(11)	9.99(10)
2009P	PGC 34730	SB	16.10(21)	15.08(09)	14.68(07)	14.43(10)	13.71(16)	13.48(14)	12.73(14)
2009Y	NGC 5728	SB	14.21(05)	11.85(10)	11.21(10)	10.84(09)	...	9.18(02)	8.48(02)

C. CSP-I HOST GALAXY PROPERTIES

We include host galaxy stellar mass of CSP-I SNe Ia as obtained using Z-PEG. Best-fit stellar mass are listed under M_{best} . Lower are upper limits of stellar masses are listed under M_{low} and M_{high} , respectively. We also include projected distance.

Table C1. Host Galaxy Properties

<i>SN Name</i>	M_{low}	M_{best}	M_{high}	<i>Projected distance</i> (kpc)
		<i>log</i> $M_{stellar}$ (M_\odot)		
2004ef	10.63	10.74	10.80	6.88
2004eo	10.97	11.16	11.29	18.92
2004ey	9.76	10.06	10.41	4.37
2004gs	10.57	10.63	10.70	8.64
2004gu	9.74	10.02	10.19	2.46
2005A	11.07	11.19	11.26	2.45
2005ag	10.84	10.90	10.95	13.38
2005al	10.40	10.49	10.63	4.32
2005am	10.68	10.83	11.26	6.67
2005be	10.22	10.40	10.53	4.85
2005bg	9.77	9.91	10.09	0.35
2005bl	10.81	11.01	11.20	8.35
2005bo	10.30	10.50	10.61	3.99
2005el	10.70	10.84	11.24	13.61
2005eq	10.40	10.56	10.65	17.61
2005hc	10.52	10.60	10.65	8.50
2005hj	9.22	9.32	9.38	3.21
2005iq	10.47	10.54	10.60	13.51
2005ir	9.07	9.23	9.43	0.43
2005kc	10.60	11.06	11.50	3.33
2005ke	10.30	10.43	10.62	5.71
2005ki	10.62	10.80	10.86	27.76
2005ku	9.96	10.04	10.10	0.85
2005lu	9.70	9.86	9.99	2.29
2005M	8.38	8.80	8.99	3.17
2005mc	10.80	10.95	11.13	3.11
2005na	10.90	10.97	11.05	3.96
2005W	9.73	9.90	10.00	10.30
2006ax	10.76	10.92	11.04	18.75
2006bd	10.60	10.77	10.80	7.82
2006bh	10.31	10.43	10.49	11.86
2006br	10.87	10.97	11.36	3.29
2006D	9.54	9.76	9.85	2.20
2006ef	10.23	10.35	10.50	9.49
2006ej	10.48	10.63	10.70	3.36
2006eq	9.79	10.19	10.65	9.94
2006et	10.70	10.80	10.88	4.71

Table C1 *continued*

Table C1 (*continued*)

<i>SN Name</i>	M_{low}	M_{best}	M_{high}	<i>Projected distance</i> (kpc)
		$\log M_{\text{stellar}} (M_{\odot})$		
2006ev	10.65	10.75	10.91	15.22
2006fw	9.26	9.42	9.61	0.71
2006gj	10.36	10.53	10.60	13.19
2006gt	9.87	9.93	9.94	15.49
2006hb	10.04	10.22	10.38	6.19
2006hx	10.12	10.31	10.44	1.91
2006is	6.68	7.10	7.41	4.47
2006kf	10.59	10.82	10.90	5.10
2006lu	10.22	10.29	10.37	5.06
2006mr	10.79	11.19	11.31	1.91
2006ob	11.08	11.26	11.33	7.08
2006os	10.66	10.81	10.87	8.19
2006py	8.91	9.10	9.20	0.08
2006X	9.06	9.33	9.51	5.09
2007af	9.23	9.52	9.98	5.25
2007ai	9.76	9.91	10.18	15.98
2007al	9.33	9.47	9.91	1.05
2007as	10.24	10.36	10.43	5.08
2007ax	10.13	10.23	10.29	0.90
2007ba	10.90	10.99	11.06	9.28
2007bc	10.65	10.73	10.78	13.88
2007bd	10.68	10.82	10.89	5.35
2007bm	10.09	10.27	10.72	1.37
2007ca	9.52	9.69	9.74	8.23
2007cg	10.33	10.37	10.43	1.92
2007hj	10.30	10.45	10.89	4.56
2007hx	10.45	10.55	10.62	20.90
2007jd	9.93	10.13	10.18	6.81
2007jg	7.95	8.10	8.22	6.34
2007jh	10.89	10.99	11.04	4.01
2007le	9.71	9.85	10.16	2.40
2007N	10.10	10.19	10.57	4.11
2007nq	11.15	11.21	11.28	19.54
2007ol	9.68	9.82	10.02	1.70
2007on	10.78	11.04	11.45	9.49
2007S	9.63	9.98	10.16	3.09
2007st	10.85	10.95	11.40	2.46
2007ux	10.23	10.30	10.34	4.23
2008ar	10.11	10.21	10.28	3.25

Table C1 *continued*

Table C1 (*continued*)

<i>SN Name</i>	M_{low}	M_{best}	M_{high}	<i>Projected distance</i> (kpc)
		<i>log M_{stellar} (M_{sun})</i>		
2008bc	10.00	10.10	10.21	5.90
2008bi	10.27	10.38	10.48	0.93
2008bq	10.74	10.82	10.91	8.59
2008bt	10.70	10.85	10.91	5.06
2008bz	10.44	10.50	10.56	7.98
2008C	10.35	10.49	10.55	0.99
2008cc	10.40	10.48	10.64	1.77
2008cd	9.37	9.54	9.67	0.84
2008cf	8.59	8.73	8.97	2.36
2008f	10.87	10.94	11.01	6.15
2008fp	10.15	10.20	10.63	2.15
2008fr	7.58	7.73	7.89	0.76
2008fu	10.66	10.72	10.80	2.70
2008fw	10.31	10.49	10.61	11.59
2008gg	10.63	10.73	10.82	22.91
2008gl	10.81	10.86	10.92	16.76
2008go	10.89	10.94	11.00	17.80
2008gp	10.64	10.73	10.79	11.84
2008hj	10.22	10.40	10.69	15.53
2008hu	10.84	10.99	11.07	39.27
2008hv	10.29	10.55	10.67	9.94
2008ia	10.54	10.77	11.23	2.24
2008O	11.12	11.33	11.59	5.39
2008R	11.15	11.25	11.31	4.00
2009aa	10.10	10.60	10.80	10.06
2009ab	10.20	10.35	10.78	8.30
2009ad	10.50	10.58	10.64	5.44
2009ag	9.99	10.20	10.60	12.79
2009al	10.66	10.72	10.77	29.32
2009cz	10.68	10.75	10.84	8.00
2009D	10.35	10.43	10.50	20.36
2009ds	10.59	10.77	10.91	4.71
2009F	10.61	10.79	11.22	3.08
2009I	10.53	10.74	10.85	6.65
2009le	10.66	10.84	11.31	5.80
2009P	9.77	9.87	9.95	1.16
2009Y	10.61	10.76	10.87	5.09

REFERENCES

- Bertin, E., & Arnouts, S. 1996, A&AS, 117, 393, doi: [10.1051/aas:1996164](https://doi.org/10.1051/aas:1996164)
- Betoule, M., Kessler, R., Guy, J., et al. 2014, A&A, 568, A22, doi: [10.1051/0004-6361/201423413](https://doi.org/10.1051/0004-6361/201423413)
- Blondin, S., & Tonry, J. L. 2007, ApJ, 666, 1024, doi: [10.1086/520494](https://doi.org/10.1086/520494)
- Brout, D., & Scolnic, D. 2020, arXiv e-prints, arXiv:2004.10206. <https://arxiv.org/abs/2004.10206>
- Burns, C. R., Stritzinger, M., Phillips, M. M., et al. 2011, AJ, 141, 19, doi: [10.1088/0004-6256/141/1/19](https://doi.org/10.1088/0004-6256/141/1/19)
- . 2014, ApJ, 789, 32, doi: [10.1088/0004-637X/789/1/32](https://doi.org/10.1088/0004-637X/789/1/32)
- Burns, C. R., Parent, E., Phillips, M. M., et al. 2018, ApJ, 869, 56, doi: [10.3847/1538-4357/aae51c](https://doi.org/10.3847/1538-4357/aae51c)
- Childress, M., Aldering, G., Antilogus, P., et al. 2013a, ApJ, 770, 108, doi: [10.1088/0004-637X/770/2/108](https://doi.org/10.1088/0004-637X/770/2/108)
- . 2013b, ApJ, 770, 107, doi: [10.1088/0004-637X/770/2/107](https://doi.org/10.1088/0004-637X/770/2/107)
- Contreras, C., Hamuy, M., Phillips, M. M., et al. 2010, AJ, 139, 519, doi: [10.1088/0004-6256/139/2/519](https://doi.org/10.1088/0004-6256/139/2/519)
- Fioc, M., & Rocca-Volmerange, B. 1997, A&A, 326, 950
- Folatelli, G., Morrell, N., Phillips, M. M., et al. 2013, ApJ, 773, 53, doi: [10.1088/0004-637X/773/1/53](https://doi.org/10.1088/0004-637X/773/1/53)
- Galbany, L., Miquel, R., Östman, L., et al. 2012, ApJ, 755, 125, doi: [10.1088/0004-637X/755/2/125](https://doi.org/10.1088/0004-637X/755/2/125)
- Galbany, L., Anderson, J. P., Sánchez, S. F., et al. 2018, ApJ, 855, 107, doi: [10.3847/1538-4357/aaaf20](https://doi.org/10.3847/1538-4357/aaaf20)
- Hamuy, M., Phillips, M. M., Maza, J., et al. 1995, AJ, 109, 1, doi: [10.1086/117251](https://doi.org/10.1086/117251)
- Hamuy, M., Trager, S. C., Pinto, P. A., et al. 2000, AJ, 120, 1479, doi: [10.1086/301527](https://doi.org/10.1086/301527)
- Hamuy, M., Phillips, M. M., Suntzeff, N. B., et al. 1996, AJ, 112, 2408, doi: [10.1086/118192](https://doi.org/10.1086/118192)
- Hamuy, M., Folatelli, G., Morrell, N. I., et al. 2006, PASP, 118, 2, doi: [10.1086/500228](https://doi.org/10.1086/500228)
- Hicken, M., Wood-Vasey, W. M., Blondin, S., et al. 2009, ApJ, 700, 1097, doi: [10.1088/0004-637X/700/2/1097](https://doi.org/10.1088/0004-637X/700/2/1097)
- Hsiao, E. Y., Conley, A., Howell, D. A., et al. 2007, ApJ, 663, 1187, doi: [10.1086/518232](https://doi.org/10.1086/518232)
- Hsiao, E. Y., Phillips, M. M., Marion, G. H., et al. 2019, PASP, 131, 014002, doi: [10.1088/1538-3873/aae961](https://doi.org/10.1088/1538-3873/aae961)
- Joyce, A., Lombriser, L., & Schmidt, F. 2016, ArXiv e-prints. <https://arxiv.org/abs/1601.06133>
- Kelly, B. C. 2007, ApJ, 665, 1489, doi: [10.1086/519947](https://doi.org/10.1086/519947)
- Kelly, P. L., Filippenko, A. V., Burke, D. L., et al. 2015, Science, 347, 1459, doi: [10.1126/science.1261475](https://doi.org/10.1126/science.1261475)
- Kelly, P. L., Hicken, M., Burke, D. L., Mandel, K. S., & Kirshner, R. P. 2010, ApJ, 715, 743, doi: [10.1088/0004-637X/715/2/743](https://doi.org/10.1088/0004-637X/715/2/743)
- Krisciunas, K., Contreras, C., Burns, C. R., et al. 2017, AJ, 154, 211, doi: [10.3847/1538-3881/aa8df0](https://doi.org/10.3847/1538-3881/aa8df0)
- Lampeitl, H., Smith, M., Nichol, R. C., et al. 2010, ApJ, 722, 566, doi: [10.1088/0004-637X/722/1/566](https://doi.org/10.1088/0004-637X/722/1/566)
- Le Borgne, D., & Rocca-Volmerange, B. 2002, A&A, 386, 446, doi: [10.1051/0004-6361:20020259](https://doi.org/10.1051/0004-6361:20020259)
- Neill, J. D., Sullivan, M., Howell, D. A., et al. 2009, ApJ, 707, 1449, doi: [10.1088/0004-637X/707/2/1449](https://doi.org/10.1088/0004-637X/707/2/1449)
- Pan, Y.-C., Sullivan, M., Maguire, K., et al. 2014, MNRAS, 438, 1391, doi: [10.1093/mnras/stt2287](https://doi.org/10.1093/mnras/stt2287)
- Perlmutter, S., Gabi, S., Goldhaber, G., et al. 1997, ApJ, 483, 565
- Phillips, M. M. 1993, ApJL, 413, L105, doi: [10.1086/186970](https://doi.org/10.1086/186970)
- Phillips, M. M., Contreras, C., Hsiao, E. Y., et al. 2019, PASP, 131, 014001, doi: [10.1088/1538-3873/aae8bd](https://doi.org/10.1088/1538-3873/aae8bd)
- Pruzhinskaya, M., Novinskaya, A., Pauna, N., & Rosnet, P. 2020, arXiv e-prints, arXiv:2006.09433. <https://arxiv.org/abs/2006.09433>
- Rana, N. C., & Basu, S. 1992, A&A, 265, 499
- Riess, A. G., Filippenko, A. V., Challis, P., et al. 1998, AJ, 116, 1009, doi: [10.1086/300499](https://doi.org/10.1086/300499)
- Rigault, M., Copin, Y., Aldering, G., et al. 2013, A&A, 560, A66, doi: [10.1051/0004-6361/201322104](https://doi.org/10.1051/0004-6361/201322104)
- Roman, M., Hardin, D., Betoule, M., et al. 2018, A&A, 615, A68, doi: [10.1051/0004-6361/201731425](https://doi.org/10.1051/0004-6361/201731425)
- Schlafly, E. F., & Finkbeiner, D. P. 2011, ApJ, 737, 103, doi: [10.1088/0004-637X/737/2/103](https://doi.org/10.1088/0004-637X/737/2/103)
- Schweizer, F., Burns, C. R., Madore, B. F., et al. 2008, AJ, 136, 1482, doi: [10.1088/0004-6256/136/4/1482](https://doi.org/10.1088/0004-6256/136/4/1482)
- Scolnic, D. M., Jones, D. O., Rest, A., et al. 2017, ArXiv e-prints. <https://arxiv.org/abs/1710.00845>
- Stritzinger, M. D., Phillips, M. M., Boldt, L. N., et al. 2011, AJ, 142, 156, doi: [10.1088/0004-6256/142/5/156](https://doi.org/10.1088/0004-6256/142/5/156)
- Sullivan, M., Conley, A., Howell, D. A., et al. 2010, MNRAS, 406, 782, doi: [10.1111/j.1365-2966.2010.16731.x](https://doi.org/10.1111/j.1365-2966.2010.16731.x)
- Tripp, R. 1998, A&A, 331, 815
- Uddin, S. A., Mould, J., Lidman, C., Ruhlmann-Kleider, V., & Hardin, D. 2017a, PASA, 34, e009, doi: [10.1017/pasa.2017.2](https://doi.org/10.1017/pasa.2017.2)
- Uddin, S. A., Mould, J., Lidman, C., Ruhlmann-Kleider, V., & Zhang, B. R. 2017b, ApJ, 848, 56, doi: [10.3847/1538-4357/aa8df7](https://doi.org/10.3847/1538-4357/aa8df7)
- Wang, L., Höflich, P., & Wheeler, J. C. 1997, ApJL, 483, L29, doi: [10.1086/310737](https://doi.org/10.1086/310737)
- Wiseman, P., Smith, M., Childress, M., et al. 2020, MNRAS, doi: [10.1093/mnras/staa1302](https://doi.org/10.1093/mnras/staa1302)